The centriculum, a membrane reticulum that surrounds *C. elegans* centrosomes, may serve as a microtubule filter

Richa Maheshwari[1], Mohammad M Rahman[1], Abigail Ruddick[1,2], Seth Drey[1,3], Robert S Mirabello[1], and Orna Cohen-Fix[1]*

[1]The Laboratory of Biochemistry and Genetics, National Institute of Diabetes and Digestive and Kidney Disease, National Institutes of Health, Bethesda MD, 20892, USA

[2]Current address: University of Oregon, Department of Biology, Eugene, OR 97403, USA

[3]Current address: University of Louisville School of Medicine, Louisville KY, 40202, USA

*Corresponding author

ornac@niddk.nih.gov,

(301) 549-2184

Running title: Centriculum as a microtubule filter

Key Words: centriculum, centrosome, *C. elegans*, microtubules, SPD-5;

Abstract

Centrosomes are cytoplasmic microtubule-nucleating structures. They are considered membraneless organelles, but in several cell types they are surrounded by ER-derived membrane. In *C. elegans* early embryos, this membrane forms a dense membrane reticulum, named the centriculum, that affects centrosome structure and microtubule nucleating capacity. The centriculum is adjacent to the centrosome's pericentriolar material (PCM) and to abundant, short peri-centrosomal microtubules. Here we show that when microtubule abundance is reduced, centriculum and PCM size decrease, while the density of the PCM protein SPD-5 increases, suggesting that the PCM can be compacted. We further show that centriculum size is determined by microtubules, and that the centriculum likely limits the length of peri-centrosomal microtubules. Finally, we find that the centriculum is more porous where spindle microtubules pass compared to where astral microtubules pass. These data are consistent with the centriculum serving as a microtubule filter, blocking the extension of most, but not all, centrosome-nucleated microtubules. Finally, if microtubule-centriculum collisions result in microtubule catastrophe, the filter function of the centriculum could also explain the high concentration of soluble tubulin at the *C. elegans* centrosome.

45 **Summary Statement**

46

47 The centriculum is a centrosome-associated membrane reticulum in *C. elegans*
48 embryos. This study shows that its size depends on microtubules and that it may act as
49 a filter, limiting microtubule growth.

50

Introduction

Centrosomes are cytoplasmic structures that nucleate microtubules, polymers made of α- and β-tubulin heterodimers that form linear, side-by-side, protofilaments, creating a hollow microtubule tube (reviewed in (Aljiboury & Hehnly, 2023)). Microtubules are polar; centrosome-nucleated microtubules have their minus (α-tubulin facing) ends embedded in the centrosome, and their plus (β-tubulin facing) ends extending away from the centrosome. Microtubules are dynamic structures that grow and shrink mainly at their plus end in a manner that is dependent on soluble tubulin concentrations and aided by microtubule associated proteins, such as motor proteins, microtubule polymerases and severing proteins, and more (reviewed in (Gudimchuk & McIntosh, 2021). In dividing cells, centrosomes nucleate microtubules that either form the mitotic spindle or extend to the cell cortex in the form of astral microtubules (reviewed in (Hoffmann, 2021)).

At the core of centrosomes are two centrioles; they are surrounded by a pericentriolar material (PCM), a proteinaceous structure whose properties are just beginning to emerge (reviewed in (Magescas *et al*, 2019; Pimenta-Marques & Bettencourt-Dias, 2020; Woodruff *et al*, 2014). The PCM is rich in coiled-coil proteins that form a lattice, or scaffold, onto which additional PCM proteins are recruited. One of the main components of the PCM in *C. elegans* is SPD-5 (Hamill *et al*, 2002), which is functionally homologous to Centrosomin/Cnn in *Drosophila* (Megraw *et al*, 2001; Megraw *et al*, 1999; Timothy *et al*, 1999) and CDK5RAP2 in vertebrates (Fong *et al*, 2008). The PCM also includes γ-tubulin (TBG-1 in *C. elegans*), which, along with associated proteins that form the γ-tubulin ring complex (γ -TuRC), serves to nucleate microtubules ((Moritz *et al*, 1995; Zheng *et al*, 1995) reviewed in (Gao *et al*, 2024)). At the onset of mitosis, the PCM increases in size in a process known as centrosome maturation ((Khodjakov & Rieder, 1999) reviewed in (Vasquez-Limeta & Loncarek, 2021)). The expansion of the *C. elegans* PCM, as measured by SPD-5 accumulation, involves the incorporation of soluble SPD-5 throughout the volume of the SPD-5 lattice (Laos *et al*, 2015; Woodruff *et al*, 2015). This process is facilitated by phosphorylation of SPD-5 by the polo-like kinase PLK-1 (Cabral *et al*, 2019; Nakajo *et al*, 2022; Rios *et al*, 2024; Woodruff *et al.*, 2015;

Wueseke *et al*, 2016). PLK-1 phosphorylation of SPD-5 is independently required to promote γ-tubulin recruitment to the PCM (Ohta *et al*, 2021). The role of PLK-1 in centrosome maturation is conserved throughout eukaryotes (Conduit *et al*, 2015; Lane & Nigg, 1996; Lee & Rhee, 2011).

Centrosomes are considered membraneless organelles, although there are numerous examples of endoplasmic reticulum (ER)-derived membrane accumulation adjacent to the centrosome in *Drosophila*, sea urchin, the fish medaka, mammalian cultured cells, and *C. elegans* (Araújo *et al*, 2023; Bergman *et al*, 2015; Bobinnec *et al*, 2003; Diaz *et al*, 2019; Harris, 1975; Karabasheva & Smyth, 2019; Rollins & Blankenship, 2023; Schlaitz, 2014; Terasaki, 2000; Waterman-Storer *et al*, 1993). This peri-centrosomal membrane was analyzed in the *C. elegans* 1-cell embryo by volume electron microscopy at 9 nm isotropic resolution and found to be made of a dense membrane reticulum, leading to its name the centriculum (Maheshwari *et al*, 2023). While the structure of peri-centrosomal membranes in other organisms has yet to be examined at this resolution, the presence of the ER curvature-inducing proteins Rtn1 and ReepB at peri-centrosomal membranes of *Drosophila* embryos (Diaz *et al.*, 2019) suggests a similar structure. In *C. elegans*, down-regulation of atlastin, which forms ER-ER junctions (Hu & Rapoport, 2016), led to an increase in centriculum size (Maheshwari *et al.*, 2023). This was accompanied by an increase in both centrosome size and the amount of PCM material (as measured by the area and total amount of fluorescently tagged PCM proteins), and increased microtubule-nucleating capacity (Maheshwari *et al.*, 2023). Likewise, in *Drosophila* embryos, alteration to ER structure, including prominent changes to the membrane surrounding centrosomes, caused defects in centrosome and spindle structure (Araújo *et al.*, 2023; Rollins & Blankenship, 2023). Thus, at least in these systems, centrosome function is affected by the membrane adjacent to it, indicating that the centrosome may not be as membraneless as previously assumed.

It is well documented that during *C. elegans* early embryogenesis, the majority of microtubules nucleated from the surface of the centrosome terminate in the vicinity of

113 the centrosome (for example, see (Albertson, 1984; Redemann *et al*, 2017) and Fig. 1A;
114 defined here as peri-centrosomal microtubules). A similar accumulation of short
115 microtubules around centrosomes is seen in embryos of medaka (Kiyomitsu *et al*,
116 2024), *Drosophila* (Rollins & Blankenship, 2023) and sea urchin (Xie *et al*, 2025), all of
117 which also have centrosome-associated ER membranes. The *C. elegans* centrosome is
118 also able to accumulate soluble tubulin at a concentration that is 10-fold higher than in
119 the cytoplasm (Baumgart *et al*, 2019). The precise mechanism that facilitates this
120 accumulation is not known. A condensate of SPD-5 with additional PCM proteins was
121 shown to concentrate soluble tubulin *in vitro* (Woodruff *et al*, 2017), although not to the
122 extent observed *in vivo* (Baumgart *et al.*, 2019). The centriculum provides an attractive
123 mechanism for these two phenomena: First, peri-centrosomal microtubule accumulation
124 could reflect collisions of a subset of microtubules with centriculum membranes that are
125 in their path and impede their elongation. In this way, the centriculum would act as a
126 microtubule filter, limiting the number of microtubules that can fully elongate. This could
127 reduce the competition for cytoplasmic tubulin pools and/or prevent the formation of a
128 poorly functioning spindle. Second, if these collided microtubules terminate at the
129 centriculum and undergo catastrophe (akin to the catastrophe that occurs when
130 microtubules encounter the plasma membrane (Bouvrais *et al*, 2021)), this could
131 provide a source for the exceedingly high soluble tubulin concentration at the
132 centrosome (Baumgart *et al.*, 2019). We therefore set out to determine the spatial
133 relationship between the centrosome, centriculum and peri-centrosomal microtubules,
134 and to examine whether the centriculum functions as a microtubule filter.
135
136 **Results**
137
138 **The spatial relationship between the centrosome, centriculum and microtubules.**
139 In our previous study ((Maheshwari *et al.*, 2023), we showed that the centriculum
140 surrounds the centrosome and the peri-centrosomal microtubules (Fig. 1A), but the
141 exact spatial relationship between the three was not quantified. To do so, we examined
142 these three structures at metaphase of the *C. elegans* 1-cell embryo, when parental
143 genomes are still encased in separate pronuclei (Fig. 1A). In 1-cell embryos, centricula

144 become visible as soon as centrosomes separate (while still associated with the male
145 pronucleus), and both centricula and centrosomes increase in size throughout the cell
146 cycle (Hamill *et al.*, 2002; Maheshwari *et al.*, 2023). Consequently, size measurements
147 must be done at the same cell cycle stage, which in our case is at metaphase. At this
148 stage, the two pronuclei are adjacent to each other, and the membrane interface
149 between them is still present (Fig. 1A). Microtubules that are nucleated from the outer
150 portion of the PCM (O'Toole *et al*, 2012) extend outwards, towards the cortex (as astral
151 microtubules), or chromosome (as spindle microtubules). However, only a fraction of
152 these microtubules extends well beyond the centrosome (Redemann *et al.*, 2017),
153 creating an accumulation of peri-centrosomal microtubules (Fig. 1A, top panel). To
154 determine the spatial relationship between the centrosome, the centriculum and the
155 peri-centrosomal microtubules, we used confocal imaging to capture the areas
156 encompassed by the structures' perimeter(s) (Fig. 1B), visualized at their largest cross
157 section; as these structures are nested within each other, the plane of their largest
158 cross-section is shared. For the centrosome, we define "PCM area" as the area
159 occupied by SPD-5, the outermost component of the PCM (Magescas *et al.*, 2019). For
160 the centriculum, visualized using fluorescently tagged SP12 (Poteryaev *et al*, 2005), we
161 defined two areas: the area encompassed by the inner perimeter of the centriculum,
162 referred to as the centriculum "void area", and the area encompassed by the outer
163 perimeter of the centriculum, referred to as "centriculum outer perimeter area", or
164 "COPA" (note that the area of the centriculum itself is the difference between COPA and
165 the centriculum void area). For peri-centrosomal microtubules, visualized using
166 fluorescently tagged α or β tubulin, we defined the area encompassed by the outer
167 perimeter of the fluorescent tubulin signal as "the peri-centrosomal microtubule area"
168 (referred to in figures as "pcMT area", for simplicity). Although peri-centrosomal
169 microtubules often appear as a ring due to the exclusion of microtubules from the center
170 of the centrosome (Strome *et al*, 2001), the difference in fluorescence between the ring
171 and its "hole" is only about 10-15% (likely due to the high concentration of soluble
172 tubulin), making "hole" size determination somewhat ambiguous. Thus, for our
173 discussion, the area occupied by peri-centrosomal microtubules includes the "hole". The
174 comparison of areas defined by the perimeters of the three structures was done using

175 pairwise combinations; imaging all three structures at once was not feasible due to a
176 weak signal when proteins were fused to blue/cyan fluorescent proteins. Parenthetically,
177 we observed that the absolute size of various structures sometimes differed between
178 strains, even when they were otherwise isogenic (see, for example, the sizes of the void
179 area and COPA in Figs. 1C and D). Thus, the relative sizes of two structures were
180 determined by comparisons within the same strain. In the next set of experiments,
181 worms were treated with control RNAi so that the measurements could be compared to
182 the various RNAi treatments, described below.
183
184 The results of the pairwise combinations are shown in Figs. 1C-E and Fig. S1B. As
185 expected, the area defined by the outer perimeter of the centriculum, COPA, was the
186 largest. The area defined by the inner perimeter of the centriculum, the void area, was
187 the smallest. The area defined by the outer perimeter of peri-centrosomal microtubules
188 was greater than the area of the PCM (using two different fluorescently tagged protein
189 combinations, see Fig. 1E and Fig S1B), and both were greater than the centriculum
190 void area, suggesting that they abut or even extend into the centriculum. For
191 microtubules, we know this to be the case based on EM tomography data (Maheshwari
192 *et al.*, 2023). Based on these data, an approximation of the overall spatial relationship
193 between the centrosome, centriculum and peri-centrosomal microtubules in wild type
194 cells is shown in Fig. 1F.
195
196 **Decrease in microtubule number or stability results in a smaller centriculum and**
197 **PCM compression.**
198 The proximity between the centrosome, centriculum and peri-centrosomal microtubules
199 raised the question of size dependency: Which of the three structures determines the
200 dimensions of one or both other structures? We previously showed that reducing the
201 levels of KLP-7, a microtubule depolymerase whose down-regulation leads to enhanced
202 microtubule outgrowth from centrosomes (Srayko *et al*, 2005), resulted in a larger
203 centriculum and a larger SPD-5 area (Maheshwari *et al.*, 2023). This suggested that
204 microtubule stability or abundance affects centriculum and/or PCM size. To further
205 examine this possibility, we examined the consequences of reduced microtubule

206 elongation or nucleation. To this end, we down-regulated by RNAi either *zyg-9* or *tbg-1*.
207 ZYG-9 is a microtubule polymerase and a homologue of *Xenopus* XMAP215 and
208 human ch-TOG. It localizes to centrosomes and the mitotic spindle (Gard & Kirschner,
209 1987; Matthews *et al*, 1998). In *Xenopus*, XMAP215 has been shown to bind free
210 tubulin dimers and catalyze their addition to the growing microtubule plus-end (Brouhard
211 *et al*, 2008). TBG-1 is the *C. elegans* γ-tubulin, which localizes to centrosomes and
212 facilitates microtubule nucleation (note that in *C. elegans*, TBG-1/ γ-tubulin is not
213 essential for microtubule nucleation at centrosomes (Hamill *et al.*, 2002; Hannak *et al*,
214 2002; Strome *et al.*, 2001). Both conditions are expected to reduce the amount of peri-
215 centrosomal microtubules (as determined by the total fluorescence of tubulin around the
216 centrosome), as is indeed the case (Fig. S1C). The area occupied by peri-centrosomal
217 microtubules was also reduced, as was the size of the centriculum (Figs. 2A-C; *zyg-9*
218 and *tbg-1* RNAi data are compared to control RNAi data also shown in Fig. 1C). These
219 results further support our conclusion that microtubule abundance and/or stability
220 affects centriculum size.
221
222 The reduction in centriculum size following *zyg-9* or *tbg-1* RNAi led us to examine what
223 happens to SPD-5 under these conditions. Using a strain expressing the SP12 ER
224 marker fused to mCherry and GFP::SPD-5, we observed that down-regulation of *zyg-9*
225 or *tbg-1* was accompanied by a decrease in centriculum size, as before (Fig. S1D), and
226 in PCM size (Figs. 2D and E). Interestingly, while the area occupied by SPD-5
227 decreased, there was no loss of SPD-5 from the PCM (Fig. 2F), and SPD-5's density in
228 the PCM increased (Fig. 2G). Overall, the increase in SPD-5 density was inversely
229 proportional to size of the centriculum void area (Fig. 2H; R^2=0.2624 for all data points).
230 This result suggests that centrosome size is affected by either microtubule abundance
231 and/or the size of the centriculum. This further suggests that the PCM is compressible
232 (see Discussion).
233
234 **The *spd-5* expansion mutant, in the presence of wild type *spd-5*, reduces overall**
235 **PCM size.**

236 The possibility that the centriculum affects centrosome size was intriguing, because the
237 centrosome is considered a membraneless organelle. In this scenario, centriculum size
238 is determined by the abundance and/or stability of microtubules, and the PCM expands
239 to the boundaries of the centriculum (Fig. 3Ai). Alternatively, however, centriculum size
240 could be determined by PCM size, while PCM size is determined by microtubules
241 abundance and/or stability (Fig. 3Aii). This latter scenario seemed less likely, because
242 PCM maturation is thought to be microtubule-independent (Hannak *et al.*, 2002;
243 Khodjakov & Rieder, 1999). Nonetheless, we needed to establish whether, in our
244 system, centriculum size was determined by the PCM or microtubules. To do so, we
245 needed a condition that differentially alters the areas occupied by the PCM vs peri-
246 centrosomal microtubules. We could then determine with which of the two centriculum
247 size correlates. This condition was met by using a *spd-5* allele that is defective in
248 expanding the SPD-5 lattice.
249
250 SPD-5 has been shown to have two separable functions: (1) centrosome maturation
251 and (2) microtubule nucleation via γ-tubulin recruitment (Ohta *et al.*, 2021). Both
252 functions are regulated by the PLK-1 kinase, which phosphorylates different residues on
253 SPD-5. Ohta et al created an RNAi-resistant *spd-5* phospho-mutant allele, *spd-5*^{exp},
254 carrying S653A and S658A substitutions, which they expressed as a transgene in the
255 presence of the endogenous wild type, RNAi sensitive, *spd-5*. As a control, wild type
256 *spd-5* was expressed as an RNAi-resistant transgene. As expected, when SPD-5^{exp} was
257 expressed as the sole SPD-5 version (i.e. endogenous *spd-5* was down-regulated by
258 RNAi), the expansion of the PCM was greatly attenuated compared to a strain
259 expressing transgenic wild type SPD-5 as its sole source of SPD-5 ((Ohta *et al.*, 2021)
260 and Figs. 3B and C). However, when transgenic SPD-5^{exp} was expressed in the
261 presence of the endogenous SPD-5 (which is untagged), transgenic SPD-5^{exp} occupied
262 a greater area than without the endogenous protein (compare transgenic GFP::SPD-
263 5^{exp} in Fig. 3C (no endogenous SPD-5) with Fig. 3D (with endogenous SPD-5); see also
264 Fig. S2A and B for more examples). This suggests that SPD-5^{exp} integrates into the wild
265 type SPD-5 lattice despite lacking two PLK-1 phosphorylation sites that contribute to
266 PCM expansion. This is consistent with in vitro findings showing that additional SPD-5

267 incorporates throughout an existing SPD-5 lattice (Woodruff *et al.*, 2017) and with
268 findings by Wueseke et al, who made similar observation with a *spd-5* allele lacking four
269 PLK-1 phosphorylation sites, including the two in SPD-5^{exp} (Wueseke *et al.*, 2016). As in
270 Wueseke et al, we also observed a good overlap between the endogenous SPD-5
271 (fused to tagRFP) and transgenic SPD-5 or SPD-5^{exp} proteins (both fused to GFP) (Fig.
272 3E), suggesting that both transgenes are integrated throughout the SPD-5 lattice.
273 Interestingly, the expression of the SPD-5^{exp} transgene in an otherwise wild type
274 background led to a smaller PCM, as judged by the areas occupied by tagRFP-tagged
275 endogenous SPD-5 (Figs. 3E-G). Furthermore, the amounts of both endogenous and
276 transgene SPD-5 at the centrosome were reduced in the presence of the *spd-5^{exp}*
277 mutant (Figs. 3 H and I). Thus, SPD-5^{exp} may act as a dominant negative, impeding the
278 ability of the SPD-5 lattice to fully expand. Alternatively, or in addition, the presence of
279 SPD-5^{exp} could have led to reduced overall levels of wild type SPD-5, as proposed by
280 Wueseke et al (Wueseke *et al.*, 2016), resulting in a smaller PCM. Note, however, that
281 the fluorescently tagged endogenous SPD-5 may exhibit a genetic interaction with the
282 expansion allele (see below).
283
284 **Centriculum size is determined by peri-centrosomal microtubules, not the PCM.**
285 Having a condition that reduced the size of the PCM, we next asked whether and how
286 the presence of the *spd-5^{exp}* mutant affected the area occupied by peri-centrosomal
287 microtubules. This was done using strains expressing wild type or expansion mutant
288 *spd-5* transgene fused to GFP in the presence of endogenous (untagged) SPD-5, and
289 α-tubulin fused to tagRFP (*tba-1::tagRFP*-T; Fig. 4A). Despite having a smaller PCM in
290 the presence of *spd-5^{exp},* as shown before (Fig. 4B), the amount of tubulin withing the
291 peri-centrosomal region was comparable in the presence of either transgene (Fig. 4C).
292 Moreover, the area occupied by peri-centrosomal microtubules did not decrease due
293 the presence of the expansion mutant transgene (Fig. 4D). As before (Fig. 1E and Fig
294 S1B), peri-centrosomal microtubules occupied a greater area than SPD-5. This area
295 differential increased in the presence of the *spd-5^{exp}* mutant (Fig. 4E) due to the smaller
296 area occupied by SPD-5 and an unchanged area occupied by peri-centrosomal

297 microtubules. Thus, peri-centrosomal microtubules were less affected by the presence
298 of the SPD-5^{exp} variant compared to the PCM.
299
300 This differential change in size of the PCM and peri-centrosomal microtubules due to
301 *spd-5^{exp}* allowed us to examine whether centriculum size follows the PCM or
302 microtubules. Specifically, by decreasing PCM size, the *spd-5^{exp}* allele increased the
303 distance (Δ) between the perimeter of the PCM and that of the peri-centrosomal
304 microtubules (Fig. 5Ai). We reasoned that measuring the effect of the *spd-5^{exp}* allele on
305 the centriculum void area (determined by the inner perimeter of the centriculum) would
306 allow us to determine if centriculum size tracks with the PCM or the peri-centrosomal
307 microtubules (Fig. 5Aii). To do so, we used the same pairwise combinations used to
308 determine the spatial relationship between the centriculum and the PCM or peri-
309 centrosomal microtubules (Fig. 1B-F), this time in the presence of the wild type or *spd-*
310 *5^{exp}* mutant transgene.
311
312 In strains expressing fluorescently tagged SP12 and TBA-1, the *spd-5^{exp}* mutant led to a
313 decrease in the area occupied by peri-centrosomal microtubules (Figs. 5B and C) but
314 not in the amount of peri-centrosomal tubulin fluorescence (Fig. S3A). This decrease in
315 peri-centrosomal microtubules area was unlike the situation in strains expressing
316 fluorescently tagged SPD-5 and TBA-1, where *spd-5^{exp}* did not affect peri-centrosomal
317 microtubule area (Figs. 4B and C). The reason for this difference is not known.
318 Nonetheless, *spd-5^{exp}* also led to a comparable decrease in centriculum size, as seen
319 by the decrease in void area (Fig. 5D) and the area encompassed by the centriculum
320 outer perimeter, COPA (Fig. S3B). Importantly, the reduction in microtubule and void
321 areas were the same (Fig. 5E, control RNAi). In contrast, when we examined the effect
322 of the *spd-5^{exp}* transgene on the centriculum in relation to the PCM using strains
323 expressing mCherry-tagged SP12 and GFP-tagged wild type or *spd-5^{exp}* transgenes,
324 the effect of *spd-5^{exp}* on the PCM was significantly greater than on the centriculum: in
325 these strains, *spd-5^{exp}* caused the area of the PCM, but not the centriculum, to shrink
326 (Figs. 5F-I, control RNAi). In fact, in several cases the size of the PCM was smaller than
327 that of the centriculum void (see negative values in Fig. 5I). Taken together, these data

328 suggest that centriculum size follows the behaviors of the peri-centrosomal microtubules
329 rather than the PCM.
330
331 To further examine the dependence of centriculum size on microtubules vs. the PCM,
332 we stabilized microtubules in strains expressing wild type or *spd-5*^{exp} transgene using
333 RNAi against *klp-7*. We reasoned that if centriculum size is determined by microtubules,
334 stabilizing microtubules in the presence of the *spd-5*^{exp} transgene might further increase
335 the distance between the PCM and the inner perimeter of the centriculum. As expected,
336 (Maheshwari *et al.*, 2023), *klp-7* RNAi led to expansion of the centriculum, PCM and
337 peri-centrosomal microtubule area (for PCM and peri-centrosomal microtubules areas,
338 compare the values in Fig. 4F (*klp-7* RNAi) with Fig. 4B and 4D (control RNAi). The
339 effect of *klp-7* RNAi on the PCM in a different strain is shown in Fig. 5G; for the
340 centriculum void area and COPA, see Fig. 5H and Fig. S3B). Following *klp-7* RNAi
341 treatment, the effect of *spd-5*^{exp} was again greater on the PCM than on the
342 pericentrosomal microtubules (Figs. 4F and G), while area differential between the
343 centriculum void area and the peri-centrosomal microtubules remained the same (Fig.
344 5E; pcMT and void areas in the presence of *klp-7* RNAi are shown in Fig. S3C).
345 However, when strains expressing the transgenic wild type or *spd-5*^{exp} mutant and
346 mCherry::SP12 were treated with RNAi against *klp-7*, a visible “gap” appeared between
347 the PCM and the inner perimeter of the centriculum (Fig. 5F, see enlarged area). While
348 *klp-7* RNAi led to an overall increase in PCM area, the presence of the *spd-5*^{exp} allele
349 led to reduced PCM area (Fig. 5G) without affecting the centriculum void area (Fig. 5H).
350 Consequently, stabilizing microtubules through *klp-7* RNAi exacerbated the difference
351 between the void area and the PCM such that in all cases, the PCM was smaller than
352 the inner perimeter of the centriculum (Fig. 5I, note negative values in the presence of
353 the *spd-5*^{exp} allele following *klp-7* RNAi). In fact, *klp-7* RNAi alone was sufficient to
354 increase the area differential between the void area and the PCM (Fig. 5I). Taken
355 together, these data suggest that the centriculum behaves the same as microtubules,
356 not the PCM, and that centriculum size is determined by microtubules.
357

358 In the experiments described above, the size of the PCM was assessed by the
359 fluorescently tagged transgenes. While there was good agreement between the areas
360 occupied by the transgenic and the endogenous SPD-5s (Fig. 3F and G), we attempted
361 to examine the spatial relationship between the centriculum and the PCM using an
362 endogenously tagged SPD-5. Unexpectedly, the *spd-5*^{exp} transgene and the
363 endogenously tagged *spd-5* exhibited a genetic interaction, resulting in abnormal
364 distribution of both proteins (Figs. 6A and Fig. S4), reminiscent of SPD-2 distribution
365 (see for example (Pelletier *et al*, 2004)). We assume that when the endogenous *spd-5*
366 was not tagged, its distribution was uniform, as judged by the uniform distribution of the
367 GFP::SPD-5^{exp} transgene, which on its own cannot expand (Fig. 3C and D and Fig.
368 S4A). However, when the endogenous *spd-5* was fused to a fluorescent protein, its
369 distribution in the presence of the transgenic *spd-5*^{exp} mutant becomes abnormal, with a
370 high concentration in the center of the centrosome, and a much lower concentration in
371 the majority of the PCM (Fig. S4B and C). Under these conditions, the distribution of the
372 GFP::SPD-5^{exp} transgene was similarly abnormal (Fig. S4B), in further support of the
373 similar distributions of the endogenous and transgene proteins. Despite this abnormal
374 distribution, we were still able to determine the area occupied by endogenously
375 expressed SPD-5, including the fainter periphery, using the same thresholding method
376 applied to all other area measurements (Fig. S4D). As before, the presence of the *spd-*
377 *5*^{exp} mutant transgene decreased the amount of SPD-5 at the centrosome, and this
378 pattern was unaffected by down-regulating *klp-7* (Fig. 6B). Also as before, down-
379 regulation of *klp-7* increased PCM area, and the presence of the *spd-5*^{exp} mutant
380 decreased PCM areas relative to the wild type transgene in both control and *klp-7* RNAi
381 conditions (Fig. 6C). Consistent with the observations above, the presence of the *spd-*
382 *5*^{exp} mutant did not reduce the size of the centriculum void volume, and down-regulation
383 of *klp-7* even increased it (Fig. 6D). Consequently, the area differential between the
384 PCM and the centriculum increased in the presence of the *spd-5*^{exp} mutant, and this
385 difference was further exacerbated when *klp-7* was down-regulated (Fig. 6E).
386
387 Taken together, these data suggest two things (Fig. 6F): First, that centriculum size is
388 likely determined by sum forces exerted on it by peri-centrosomal microtubules.

389 Second, because the area occupied by pericentrosomal microtubules change little or
390 none when the PCM “shrinks” due to the presence of the *spd-5*^{exp} mutant, and because
391 microtubules nucleate from the surface of the PCM, our data suggest that the length of
392 pericentrosomal microtubules is not an inherent property of these microtubules,
393 because their length, from the surface of the PCM to the inner perimeter of the
394 centriculum, must be different in wild type vs *spd-5*^{exp} expressing cells (Fig. 6F). Rather,
395 our data suggest that the majority of pericentrosomal microtubules extend from the
396 surface of the PCM until they encounter the centriculum, where most of them terminate
397 due to obstruction by the centriculum membrane; only a small fraction can extend past
398 the centriculum to form astral or spindle microtubules. As such, the centriculum may
399 serve as a microtubule filter, a possibility that is explored next.
400
401 **Centriculum porosity correlates with the ability of microtubules to traverse the**
402 **centriculum.**
403 As noted above, two types of centrosome-nucleated microtubules extend beyond the
404 centriculum: astral microtubules, which extend towards the cell cortex, and spindle
405 microtubules, which extend towards chromosomes. The density of spindle microtubules
406 is much greater than astral microtubules (Fig. 7A, metaphase). Spindle microtubules are
407 only evident in metaphase; prior to that, only astral microtubules can be observed
408 outside the centriculum, and no microtubules have entered the pronuclei (Fig. 7A,
409 prophase). If the centriculum serves as a microtubule filter, we would expect that at
410 metaphase, the centriculum would be more porous on the side facing the chromosomes
411 vs. the side facing the cortex. To examine this possibility, we measured the effective
412 pore size that is available for microtubules nucleated at centrosomes to pass through
413 the centriculum using volume electron microscopy data acquired via focused ion beam-
414 scanning electron microcopy (FIB-SEM; (Maheshwari *et al.*, 2023)).
415
416 We created a fiducial in the center of segmented metaphase centricula, and imaged a
417 portion of the centriculum, from that fiducial, against a black background (Fig. 7B and C;
418 images were taken from within the centrosome towards either the cortex or the
419 chromosomes). Qualitatively, it already appeared that the holes on the chromosomal

side are larger than those on the cortical side (compare the two central panels, chromosome-facing 1 and 2, to the side panels, cortex-facing 1 and 2). To maximize having the openings imaged *en face*, the angles between the center line and the top or bottom of any image were kept to a minimum (for cortex facing areas: 23.8° ± 2.82°, average and standard deviation, n=6; for chromosome facing areas: 22.8° ± 2.23°, average and standard deviation, n=6). We then determined the area of each opening, defined as “hole”, that can be seen through the centriculum. Considering that the diameter of a microtubule is ~25 nm, the area of the smallest hole through which a microtubule can pass would be 490 nm^2 (π x 12.5^2) and probably larger since most holes are not perfect circles. The fraction of cortex-facing centriculum area that was open, namely the sum of all hole areas out of the total area imaged, was 7.85 ± 1.66% (n=6, from 3 centricula), while on the chromosome side it was significantly greater: 20.66 ± 3.75%, (n=6 from 3 centricula; p=0.009 as determined by chi square test), consistent with the chromosome-facing side of the centriculum having larger opening. In the case of cortex-facing holes, the cross sections of 61.34% of the holes, accounting for 7.5% of the total open area, were below 500 nm^2, likely too small to allow for a microtubule to pass (Fig. 7D and E). The percent of chromosome facing holes that had a cross section below 500 nm^2 was 41.88%, and this accounted for only 1.4% of the total open area on the chromosomal side (Fig. 7D and E). On the other side of the hole-size spectrum, 11.56% of the open area facing the cortex were from holes that were larger than 10,000 nm^2 (0.8% of all holes), compared to 74.52% on the chromosome-facing side (9.1% of all holes) (Fig. 7E). Thus, the centriculum side facing the chromosomes, through which spindle microtubules pass, is significantly more porous than the side facing the cortex, where astral microtubules pass. Whether the different degrees of porosity are caused by centriculum geometry or by properties of spindle microtubules remains to be determined (see Discussion).

Given that only a small fraction of the centriculum area facing the cortex is available for the microtubules to go through, and the fact that the thickness of centriculum at metaphase is around 1 µm (Maheshwari *et al.*, 2023), we predicted that the microtubules that become fully elongated astral microtubules are those that take the

451 shortest path through the centriculum, and are thus less likely to encounter centriculum
452 membrane. To test this hypothesis, we used ER tomography datasets of 1-cell embryos
453 at metaphase (Maheshwari *et al.*, 2023; Redemann *et al.*, 2017) and measured the
454 angle of microtubules as they pass the inner perimeter of the centriculum relative to the
455 radial vector, the line that is perpendicular to the tangent line (Fig. 8A). The shortest
456 path through the centriculum would be that of the radial vector (angle= 0°); increasing
457 angles between a microtubule path and the radial vector would mean longer paths
458 through the centriculum. We then determined whether the microtubule passed through
459 the centriculum (denoted as “continuing”) or whether the microtubule terminated within
460 the centriculum (denoted “stopped”). On the cortex-facing side, we measured angles for
461 113 microtubules, of which 21 continued (18.6%), and on the chromosome-facing side
462 we measured angles for 146 microtubules, of which 40 continued (27.4%). In both
463 cases, the distribution of angles of microtubules that passed all the way through the
464 centriculum was significantly narrower, and closer to the radial vector, than the range of
465 angles for microtubules that ended within the centriculum (Fig. 8B). Nonetheless, our
466 data suggest that the centriculum serves as a passive microtubule filter, blocking most
467 microtubules from extending past the centriculum.
468
469 To form a spindle, microtubules must enter the space around the chromosomes. Prior to
470 metaphase, an intact nuclear envelope prevents centrosome-nucleated microtubules
471 from entering the nucleoplasm. Just before metaphase, two events take place: the
472 nuclear envelope loses its integrity specifically next to centrosomes (Hachet *et al*,
473 2012), and the centriculum fuses with the nuclear membrane (Maheshwari *et al.*, 2023).
474 In this regard, the larger hole size of the centriculum on the chromosomal side is
475 unlikely to be the only reason why spindle microtubule density is greater than that of
476 astral microtubules. At prometaphase, the percent of open centriculum area (14.64 ±
477 4.14%, n=6 from 3 centricula), distribution of hole size, and percent area per hole size
478 (Fig. S5A and B) on the chromosomal side of the centriculum were similar to those of
479 metaphase centricula. Effectviely, however, the number of holes available for
480 microtubules to reach the chromosomes is significantly smaller, because at
481 prometaphase, remnants of the nuclear membrane are still present, creating an

482 additional barrier for microtubules to enter the nucleoplasm (Fig. 8C, note the presence
483 of nuclear membrane (in green) masking many of the openings). At prometaphase the
484 centriculum is adjacent to the nuclear membrane, with a few possible contact sites (see,
485 for example, Fig. 8D), but there are no membrane junctions that indicate actual fusion.
486 In contrast, at metaphase, the centriculum is completely fused with the remnants of the
487 nuclear membrane (Maheshwari *et al.*, 2023), possibly in an atlastin-dependent manner
488 ((Araújo *et al.*, 2023) and see below). Therefore, at metaphase, there are no other
489 membranes between the centriculum and the chromosomes. Thus, the fusion of the
490 centriculum and mitotic remnants of the nuclear membrane may reduce membrane
491 barriers in the process of spindle formation.
492
493 A further indication that centriculum-nuclear membrane fusion is important for spindle
494 microtubule formation is the state of metaphase 1-cell embryos following atlastin down-
495 regulation. Atlastin is a GTPase needed for the fusion of ER tubules (Hu & Rapoport,
496 2016; Orso *et al*, 2009). We down-regulated atlastin using a degron construct, under
497 conditions that partially lower the amount of atlastin in the embryo (Maheshwari *et al.*,
498 2023). Under these conditions, for unknown reasons, pronuclei have difficulties aligning,
499 and they sometimes fuse with only one of the two centricula (Fig. 8E, see pronuclei
500 marked in blue asterisks in panels i and iii), leading to the formation of monopolar
501 spindles in those pronuclei. Centricula at metaphase are normally fused to both
502 pronuclei, resulting in two dense clusters of spindle microtubules on either side of the
503 membrane between the two pronuclei (for example, see Fig. 7A). However, when *atln-1*
504 is down-regulated, a centriculum may fuse with only one of the two pronuclei (Fig. 8E,
505 red arrows). Under these conditions, dense microtubules can be observed only where
506 the centriculum is fused to the pronuclei, while the rest of the centriculum is surrounded
507 by lower density, astral microtubules (Fig. 8E and enlarged areas from panels iii and iv).
508 This suggests that robust microtubule elongation past the centriculum to form the
509 spindle's dense microtubule array can only happen once the centriculum fuses with a
510 pronucleus. Taken together, we proposed that formation of high-density microtubules on
511 the chromosome-facing side of the centriculum is facilitated by two processes: the

presence of large openings that traverse the centriculum, and the fusion of the centriculum with remnants of the nuclear membrane.

517 **Discussion**

518 In this study, we tested the hypothesis that the centriculum acts as a partial barrier, or
519 filter, preventing the extension of some, but not all, centrosome nucleated microtubules.
520 Our measurements show that the PCM and peri-centrosomal microtubules either abut
521 or slightly penetrate the inner perimeter of the centriculum (Fig. 1). We further observed,
522 both here and in our previous study, that changing microtubule stability or number
523 affects both PCM size and centriculum size ((Maheshwari *et al.*, 2023) and Figs 2, 5G-I,
524 6 and Figs. S1 C and D, and S3)). This suggested that microtubules affect centriculum
525 size either directly, potentially by exerting force on the centriculum and thus determining
526 its size, or indirectly, by affecting PCM size, which in turn affects centriculum size. To
527 gain insight into the spatial dependencies of these three structures, we used a *spd-5*
528 allele, *spd-5*^{exp}, that is defective in PCM expansion (Ohta *et al.*, 2021). Expressing both
529 *spd-5*^{exp}, as a transgene, and the endogenous wild type *spd-5* resulted in a smaller
530 PCM. An inhibitory effect by SPD-5 mutant proteins on the SPD-5 lattice has been
531 observed previously: Nakajo et al. observed this phenotype with a 272 amino acid C-
532 terminal deletion, which did not encompass the residues mutated in SPD-5^{exp} (Nakajo *et*
533 *al.*, 2022), while Wueseke et al. observed it with a SPD-5 variant lacking four PLK-1
534 phosphorylation sites, SPD-5^{4A}, including the two in SPD-5^{exp} (Wueseke *et al.*, 2016).
535 Rios et al found that PLK-1 phosphorylation of SPD-5 reduces intramolecular
536 interactions, allowing these domains to interact intermolecularly (Rios *et al.*, 2024). We
537 therefore propose that the SPD-5^{exp} variant acts as a dominant negative by
538 incorporating into the SPD-5 lattice but not contributing fully to intermolecular
539 connections, thereby impeding lattice expansion. Alternatively, or in addition, the
540 presence of transgenic mutant *spd-5* may have led to reduced levels of endogenously
541 expressed *spd-5* (Wueseke *et al.*, 2016), thus resulting in a smaller PCM.
542
543 Importantly, expressing both transgenic *spd-5*^{exp} together with the endogenous wild type
544 *spd-5* resulted in a smaller PCM without reducing the area occupied by the peri-
545 centrosomal microtubules (Fig. 4A-D). The same was true when worms were treated
546 with RNAi against *klp-7*, which stabilizes microtubules: while the areas occupied by the
547 PCM and peri-centrosomal microtubules was overall greater due to *klp-7* down-

548 regulation (Maheshwari *et al.*, 2023), only PCM area, but not peri-centrosomal
549 microtubule area, was affected by the presence of SPD-5^{exp} (Fig 4F). In other words,
550 expression of the *spd-5^{exp}* allele led to a greater difference in the areas occupied by
551 peri-centrosomal microtubules compared to the PCM (Fig 5E and G). This experimental
552 setup allowed us to address two questions: the first was what determines centriculum
553 size. By examining centriculum size relative to the PCM vs per-centrosomal
554 microtubules in the presence of *spd-5^{exp}*, we showed that the centriculum correlates
555 with microtubules, not the PCM (Fig 5). In fact, under *klp-7* RNAi treatment, a gap was
556 visible between the inner perimeter of the centriculum and the PCM (Fig 5F). The
557 increase is distance between the centriculum and the PCM was true regardless of
558 whether PCM area was determined using the transgene or endogenous SPD-5 (Fig 6
559 E). Thus, our data are consistent with the possibility that centriculum size is determined
560 by microtubules, not by the PCM. This further suggests that PCM size could be affected
561 by the size of the centriculum, such that, for example, when the centriculum is unusually
562 small due to reduced microtubule number or stability, the centriculum could lead to PCM
563 compaction (Fig 2). This is an intriguing possibility, as it suggests that the PCM lattice is
564 malleable, able to expand or fold inwards in response to forces acting upon it, akin to a
565 Hoberman Sphere (https://www.hoberman.com/portfolio/hoberman-sphere-toy/). That
566 the PCM is malleable was also proposed by Laos et al, who noted that the PCM lattice
567 *in vivo* can grow by incorporating SPD-5 anywhere within the lattice (Laos *et al.*, 2015).
568 This property could contribute to the PCM's ability to deform in response to forces
569 exerted on it by astral microtubules (Enos *et al.*, 2018), where the PCM could stretch
570 rather than break. This property, known as ductility, was also proposed by Mittasch et al
571 based on the PCM's deformability during anaphase in response to external forces
572 (Mittasch *et al.*, 2020).
573
574 The second question this experimental set up allowed us to address is whether peri-
575 centrosomal microtubules are short due to an inherent property. Numerous in vitro
576 studies, using tubulin concentrations that were significantly lower than in the 1-cell *C.*
577 *elegans* embryo, have examined microtubule length either directly or indirectly, and in
578 none of them were microtubules as short as the *C. elegans* 1-cell peri-centrosomal

microtubules (Arnal *et al*, 2004; Belmont *et al*, 1990; Chrétien *et al*, 1995; Farrell *et al*, 1987; Fygenson *et al*, 1994; Gould & Borisy 1977; Grego *et al*, 2001; Kuriyama & Borisy, 1981; Mitchison & Kirschner, 1984; Verde *et al*, 1990), suggesting that something is preventing the extension of peri-centrosomal microtubules. Ideally, we would have liked to remove the centriculum entirely and examine the effect on peri-centrosomal microtubule length. Unfortunately, we have yet to identify a condition that eliminates the centriculum. Nonetheless, the *spd-5*^{exp} allele created a condition where limits to peri-centrosomal microtubule length could be examined. Microtubules are nucleated from the outer portion of the PCM. In the presence of the *spd-5*^{exp} allele, the PCM is smaller, but the area occupied by peri-centrosomal microtubules, as determined by the outer periphery of this structure, remains unchanged (Fig 4B, D and F). This suggests that in the presence of the *spd-5*^{exp} allele, peri-centrosomal microtubules are longer than in the control (Fig 6F). If the length of peri-centrosomal microtubules were a function of an inherent property of these microtubules, the area occupied by these microtubules would have been smaller in the presence of SPD-5^{exp}. Thus, we propose that the accumulation of peri-centrosomal microtubules is a consequence of the presence of the centriculum, which blocks the extension of a subset of microtubules that are nucleated by the centrosome. While elongating microtubules have the capacity to distort a membrane sheet (for example, see (Zimmerman & Chang, 2005)), we propose that the reticular nature of the centriculum, creating a membrane lattice, allows it to resist forces exerted on it by microtubules. Consistent with this possibility, the microtubules that manage to pass through the centriculum take, on average, a shorter route than microtubules that stop within the centriculum (Fig 8A and B). If microtubules were agnostic to the presence of the centriculum, there would be no difference in the angle relative to the radial vector of microtubules that terminate within the centriculum and those that extend past it. A similar accumulation of peri-centrosomal microtubules was observed in other organisms that also have peri-centrosomal ER accumulation (Kiyomitsu *et al.*, 2024; Rollins & Blankenship, 2023; Xie *et al.*, 2025).

While the centriculum may act as a barrier to the extension of peri-centrosomal microtubules, it is still permissive to extension of astral and spindle microtubule

610 extension. The density of microtubules extending toward the chromosomes by far
611 exceeds the density of microtubules extending toward the cortex (Figs. 1A and 7A). This
612 difference in density correlates with the size of centriculum “holes” and the overall open
613 area, which is significantly greater on the side of the centriculum that faces the
614 chromosomes compared to the side facing the cortex (Fig 7). We imagine two non-
615 mutually exclusive reasons why centriculum holes are larger on the side facing the
616 chromosomes: first, prior to metaphase, this side of the centriculum is adjacent to the
617 pronuclear membrane and is not as wide as the parts facing the cytoplasm (Maheshwari
618 *et al.*, 2023), perhaps due to a spatial restriction of ER-derived membrane
619 accumulation. If we assume that the centriculum is a passive barrier, the wider it is, the
620 more microtubules it will block from extending. Second, the centriculum is likely a
621 dynamic structure, much like the rest of the ER. At metaphase, microtubules that reach
622 the chromosomes are stabilized, likely restricting the ability of the centriculum to
623 remodel around these microtubules. Under these conditions, it is possible that additional
624 microtubules can pass alongside the stable microtubule, further reducing the ability of
625 the centriculum to remodel at that site and establishing a “hole” whose size may
626 continue to increase. Consistent with this possibility, we observe a high density of
627 microtubules extending past the centriculum only after the centriculum fuses with
628 remnants of the pronuclear membranes (Fig 8E). This explanation may also apply to
629 cortical microtubules, which although not stabilized, may still promote the passage of
630 additional microtubules through the centriculum alongside them. Indeed, the distribution
631 of astral microtubules is not uniform (Fig. 7A), perhaps due to the filter properties of the
632 centriculum.
633
634 Taken together, we propose that the centriculum acts as a partial barrier, or filter, of
635 centrosome-nucleated microtubule, blocking the extension of many centrosome-
636 nucleated microtubules, thereby limiting the number of astral and spindle microtubules.
637 This may limit competition for limited cytoplasmic pools of soluble tubulin, which might
638 only be sufficient for a limited number of astral microtubules to extend all the way to
639 cortex. Likewise, an over-abundance of microtubules might interfere with proper spindle
640 formation or function. Moreover, the termination of peri-centrosomal microtubules at the

641 centriculum would likely result in microtubule catastrophe, creating an environment of
642 high tubulin concentration, as observed by Baumgart et al (Baumgart *et al.*, 2019); the
643 free tubulin is then captured by the PCM, which is capable of concentrating tubulin *in*
644 *vitro* (Woodruff *et al.*, 2017). Thus, the barrier properties of the centriculum could explain
645 both the accumulation of short peri-centrosomal microtubules and the accumulation of
646 soluble tubulin at the centrosome.
647
648 To date, the only centrosome-adjacent membrane that has been examined at
649 nanometer resolution is the *C. elegans* centriculum. Similar membrane structures,
650 however, have been observed in other cell types (Araújo *et al.*, 2023; Bergman *et al.*,
651 2015; Bobinnec *et al.*, 2003; Diaz *et al.*, 2019; Harris, 1975; Karabasheva & Smyth,
652 2019; Terasaki, 2000; Waterman-Storer *et al.*, 1993). In many cases, centrosome-
653 associated membranes are most prominent in the embryo (e.g. *C. elegans*, *Drosophila*
654 and sea urchin). Early embryos typically contain stores of protein and mRNA that are
655 used in the first few embryonic divisions, before the onset of zygotic expression. The
656 centriculum and other centrosome-associated membranes may help limit the number of
657 astral microtubules under conditions where microtubule nucleating capacity exceeds the
658 needs of the embryo. Given the overall conservation in centrosome and ER-associated
659 proteins, it is possible that centrosome structure and function in additional cell types are
660 also affected by an adjacent ER-derived membrane reticulum. If this is the case, then
661 the repertoire of proteins and processes that affect centrosome function is broader than
662 previously appreciated, and defects in these proteins or processes might be a basis for
663 centrosome-related human disease.
664
665

666 **Materials and Methods**
667
668 ***C. elegans* strains**
669
670 The *C. elegans* strains used in this study were derived from the N2 strain (Bristol;
671 (Brenner, 1974) and are listed in Table S1. Strains were maintained at 20°C on OP50
672 unless treated with RNAi (see below), using standard methods (Brenner, 1974).
673
674 **Manipulations of gene and protein expression**
675 ***Feeding RNAi***
676 *E. coli* RNAi feeding clones against *smd-1* F47G4.1, *klp-7* K11D9.1, *zyg-9* F22B5.7 and
677 *tbg-1* F58A4.8 were from a *C. elegans* RNAi feeding library (Open Biosystems,
678 Huntsville, AL). For *klp-7*, *tbg-1*, *zyg-9* or *smd-1* (control (Golden *et al*, 2009)) feeding
679 RNAi treatments, a 5 ml Luria Broth (LB) with 50 µg/ml ampicillin (Sigma Aldrich, Cat #
680 A9518) were inoculated using 1:100 dilution of an overnight saturated culture (at 37°C)
681 of *E. coli* expressing dsRNA of the gene of interest. Once the culture grew to OD_{600} of
682 around 0.5 (~ 4 h at 37°C), 0.5 M IPTG (Sigma Aldrich, Cat # I6758, 1 mM final
683 concentration) was added to induce the bidirectional transcription of the relevant gene
684 for another 4 h. The culture was centrifuged at 5000 g for 5 min at room temperature,
685 and the pellet was resuspended in 1 ml of fresh LB + ampicillin (50 µg/ml) media. 200 µl
686 of this culture were spread on each RNAi plate (MYOB with 4 mM IPTG and ampicillin
687 50 µg/ml). For feeding RNAi treatment, 20-40 L4-stage larvae were transferred to RNAi
688 plates at 20°C, and after 48 h (for *klp-7*), or 24 h (for *tbg-1* and *zyg-9*), the RNAi treated
689 worms were dissected on a glass slide, mounted on a 2% agar pad, and imaged as
690 described below. Control RNAi treatments (*smd-1*) were done for the same amount of
691 time as the experimental ones.
692
693 ***dsRNA injection RNAi***
694 RNAi against *spd-5* was done using injection of double stranded RNA (dsRNA). A region
695 of *spd-5* from 500-949 bp, was PCR amplified from N2 genomic DNA using
696 oligonucleotides containing T7 or T3 promoter sequence. The amplified region was gel
697 purified and then reamplified with the same PCR primers. The PCR product was purified
698 using the Qiagen MinElute Reaction Cleanup Kit (Cat # 28206). To prepare the RNA for

699 injection, in vitro RNA synthesis was carried out using MEGAscript™ T7 Transcription
700 Kit (Invitrogen Cat # AM1333; for forward strand) and MEGAscript™ T3 Transcription Kit
701 (Invitrogen Cat # AM1338; for the reverse strand) followed by purification using
702 Phenol:CHCl3:Isoamyl Alcohol (invitrogen Cat # 15593031; 25:24:1, v/v) and
703 precipitated using 100% ethanol. The RNA pellet was dissolved in water. To prepare
704 dsRNA, an equal amount (2 µg/µl) of both the ssRNAs were mixed and incubated at
705 85°C for 3 minutes in an aluminum heat block incubator followed by slow cooling to
706 room temperature for annealing. Injection of dsRNA was done according to Ohta
707 laboratory protocol (Ohta *et al.*, 2021). L4s (15-20 worms) were injected with ~1 µg/µl
708 dsRNA. These worms were maintained at 16°C for 48 h prior to live imaging of early
709 embryos by confocal microscopy.
710
711 ***Auxin-mediated degradation***
712 Auxin mediated degradation of ATLN-1 was done as described previously (Maheshwari
713 *et al.*, 2023). The *atln-1* gene was tagged with an auxin-inducible degron tag (atln-
714 1::degron) in cells expressing TIR1, an exogenous F-box protein. Worms were
715 transferred to bacteria seeded indole-3 acetic acid (IAA, Alfa Aesar Cat # A10556)
716 plates (MYOB plates with 4 mM IAA) for ~20-25 minutes, and embryos were imaged
717 immediately thereafter, as per Zhang et al 2015 (Zhang *et al*, 2015).
718
719 **Confocal microscopy**
720 ***Imaging***
721 Images were taken using a Nikon confocal Ti2 with Yokagawa CSU-X1 spinning disk
722 and a photometrix Prime 95B camera using a Nikon water/oil 60X 1.2-NA Apo Plan
723 objective. Images were captured using Nikon Elements software version 5.20.00. For
724 imaging, embryos were mounted on 2% agarose pads prepared in standard M9 buffer.
725 Images were taken at z=1 µm intervals unless otherwise mentioned.
726
727 ***Image analysis***
728 All images were analyzed using Fiji (Schindelin *et al.*, 2012), http://imagej.nih.gov/ij).
729

730 **Measurements:**

731 ***Measurement of areas and amount***

732 To compare between structures, images were taken by confocal microscopy as
733 described above, and the comparisons between relevant structures were done at their
734 midplane, where these structures is at its largest cross section. Since the centriculum,
735 peri-centrosomal microtubules and centrosome are symmetrically nested within each
736 other, the midplane of any two structures was at the same image plane. To determine
737 the area of a given structure, the boundaries of structure were roughly traced. In the
738 case of the PCM this involved tracing the outer perimeter of SPD-5. For the centriculum
739 and peri-centrosomal microtubule ring, this involved tracing both the inner and outer
740 perimeters of the ring, excluding nuclear membranes and spindle microtubules,
741 respectively, resulting in a toroidal shape (Fig. S1A). For each traced area, the
742 minimum (min) and mean fluorescent values were determined. Empirically, the most
743 consistently faithful representation of the different structures' areas was by using the
744 formula (mean+min)/2 to set the lower threshold value, and Max (maximum threshold,
745 found in same measurement results FIJI that also included mean and minimum intensity
746 values) to set the upper threshold. These values were entered into the threshold
747 function of FIJI, resulting in consistently accurate representation of the structure's area
748 (in the case of the microtubule ring, since the difference in intensity between the ring
749 and its center is only about 15%, this method did not result in a ring but rather a solid
750 round area) (Fig. S1A). Of note, while in the present study the min/mean ratios were
751 determined for each structure in each image, these values are highly consistent, and
752 once determined can be applied to a given structure. For example, the min/mean ratio
753 of the traced centriculum region for mCherry::SP12 were 0.79 $\pm$ 0.03 (control RNAi;
754 n=16) and 0.76 $\pm$ 0.04 (*klp-7* RNAi; n=16); for GFP:: SP12 they were 0.75 $\pm$ 0.05
755 (control RNAi; n=16) and 0.74 $\pm$ 0.03 (*klp-7* RNAi; n=20).

756 For the PCM and peri-centrosomal microtubules, the area and total fluorescence (Raw
757 Intensity) were measured in the thresholded region using the analyze > measure
758 function in FIJI. For the centriculum, the inner perimeter of the thresholded centriculum
759 was selected using wand tool in FIJI to get the void area. For the area defined by the

760 outer perimeter, we traced the thresholded outer edge of the centriculum thereby
761 determining the area bound by the centriculum's outer perimeter.
762
763 ***Microtubule angle measurement***
764 In a zoomed-in screenshot of a 240-slice-thick section of the tomography data
765 containing the area of interest (Maheshwari *et al.*, 2023; Redemann *et al.*, 2017)
766 originally from Amira, two straight lines were drawn, marking the approximate interior
767 and exterior edges of the centriculum (Fig. 8A; while the edges of the centriculum are
768 curved, at this resolution the edge approaches a straight line that represents the tangent
769 line of the centriculum edge). Microtubules that crossed the interior edge were traced
770 using the straight line tool in FIJI. If a microtubule continued beyond the exterior
771 boundary line of the centriculum, it was categorized as a "continued MT." Microtubules
772 that stopped before reaching the exterior boundary were categorized as "stopped MT."
773 To ensure that microtubules defined as "stopped" did not continue outside the range of
774 the slice that was being analyzed, screenshots were taken of 300 slices above and
775 below the same area of the initial screenshot. These images were used to determine
776 whether the traced microtubules continued in another plane. Those that did not continue
777 on either the above or below slice set were considered stopped.
778
779 To measure microtubule angles, the angle between the inner centriculum edge line (the
780 tangent line) and the microtubule line was determined. This angle was then subtracted
781 from 90 degrees. The resulting value represents the angle between the microtubule and
782 the perpendicular to the tangent line, also referred to as the normal line (Fig. 8A).
783
784 **Focused-Ion beam scanning electron microscope (FIB-SEM) imaging**
785 The FIB-SEM data used in this study was previously published (Rahman *et al*, 2020).
786 3D segmentation of centriculum structure were done as previously published (Rahman
787 *et al.*, 2020) using Amira 6 (version 3D 2022.2, FEI/Thermo Fisher Scientific) default
788 general scheme to segment selected ROI in a semi-autonomous method. Briefly, first,
789 we selected centriculum membranes using a threshold followed by at least three rounds
790 of manual inspection (slice by slice through X, Y, and Z separate planes) to remove

791 incorrect segments and add unsegmented membranes to the final membrane volume
792 (Maheshwari *et al.*, 2023; Rahman *et al.*, 2020).
793
794 To measure the size of centriculum openings (namely open space between reticular
795 membranes that extend all the way through the centriculum), we placed fiducials (on the
796 same plane) next membrane edges on the pronuclear and cortical size of the
797 centriculum. We took TIFF screenshots of the centriculum membrane from behind a
798 central fiducial (i.e., equal distance from the pronuclear and cortical centriculum
799 membrane fiducials) placed on the same plane as perinuclear/cortical fiducials. For
800 each TIFF image, we determined a scale bar separately by marking 11 consecutive
801 pixels as 100 nm. We measured the size of each hole using the threshold-based
802 selection and area measurement tool in Fiji (version 2.14.0/1.54f). To ensure that the
803 centriculum segments in these images are *en face*, we restricted the angle between the
804 center plane and the top and bottom of each image to less than 30°. The actual angle
805 was determined by drawing straight lines from the central fiducial to fiducials that were
806 placed on the top bottom edges of each image. Next, we took TIFF images of the
807 perpendicular view of the above-mentioned lines and utilized the angle measurement
808 tool in Fiji.
809
810 **Statistical analysis**
811 All analyses were done using GraphPad Prism (GraphPad Prism [Version 10.1.1
812 (270)]). For comparisons between two normally distributed samples, unpaired t-tests
813 were used; otherwise, a two-tailed Mann-Whitney test was used as a non-parametric
814 test. For comparison between multiple datasets, one-way ANOVA non-parametric
815 Kruskal-Wallis test with correction for multiple comparisons was used. The statistical
816 tests used, the number of samples analyzed, and the p-values are indicated in the
817 Figure legends. The criterion for statistical significance was set at $p < 0.05$. Results in all
818 graphs are represented as mean ± standard deviation unless indicated otherwise. The
819 binned frequency distribution graphs in Fig. 7, 8 and Supplemental Figure S3 were done
820 using Microsoft excel. The bin width was set at 500 nm^2 up to 1000 nm^2 then from 1001
821 to 10000 the data were binned at every 1000 nm^2 with overflow bin set at >10000 nm^2.

AI use

AI was not used in any part of this study or manuscript preparation.

Acknowledgments

We thank Karen Oegema (UC San Diego), Jessica Feldman (Stanford University), Jon Audhya (University of Wisconsin-Madison) and the *Caenohrabditis* Genetics Center for strains. We thank Kevin O'Connell (NIH, NIDDK), Antonina Roll-Mecak (NIH, NINDS), Gunar Fabig (University of Dresden) and Alexey Khodjakov (Wadsworth Center, New York State Department of Health) for helpful discussions. We also thank Kevin O'Connell for comments on the manuscript. We thank Kedar Narayan for support in obtaining FIB-SEM data. R.M., M.M.R., A.R., S.D., R.S.M. and O.C-F. were supported by an NIDDK intramural grant to O.C-F., DK069012-18.

This research was supported by the Intramural Research Program of the National Institute of Diabetes and Digestive and Kidney Diseases (NIDDK) within the National Institutes of Health (NIH). The contributions of the NIH authors were made as part of their official duties as NIH federal employees, are in compliance with agency policy requirements, and are considered Works of the United States Government. However, the findings and conclusions presented in this paper are those of the authors and do not necessarily reflect the views of the NIH or the U.S. Department of Health and Human Services

Author contribution: The premise of this study was conceptualized by R.M., M.M.R and O.C-F. Experiments were designed, executed and analyzed by R.M., M.M.R, A.R., S.D. R.S.M, and O.C-F. Methodology was developed by R.M., M.M.R, A.R., and S.D. O.C-F supervised the project and wrote the original draft. All authors reviewed and commented on the original draft as well as all other manuscript iterations and accepted the final manuscript.

Disclosure of competing interests

The authors declare that there are no competing interests.

References

Albertson DG (1984) Formation of the first cleavage spindle in nematode embryos. *Dev Biol* 101: 61-72

Aljiboury A, Hehnly H (2023) The centrosome - diverse functions in fertilization and development across species. *J Cell Sci* 136: jcs261387

Araújo M, Tavares A, Vieira DV, Telley IA, Oliveira RA (2023) Endoplasmic reticulum membranes are continuously required to maintain mitotic spindle size and forces. *Life Sci Alliance* 6: 202201540

Arnal I, Heichette C, Diamantopoulos GS, Chrétien D (2004) CLIP-170/Tubulin-Curved Oligomers Coassemble at Microtubule Ends and Promote Rescues. *Curr Biol* 14: 2086-2095

Baumgart J, Kirchner M, Redemann S, Bond A, Woodruff J, Verbavatz J-M, Jülicher F, Müller-Reichert T, Hyman AA, Brugués J (2019) Soluble tubulin is significantly enriched at mitotic centrosomes. *J Cell Biol* 218: 3977-3985

Belmont LD, Hyman AA, Sawin KE, Mitchison TJ (1990) Real-time visualization of cell cycle-dependent changes in microtubule dynamics in cytoplasmic extracts. *Cell* 62: 579-589

Bergman ZJ, Mclaurin JD, Eritano AS, Johnson BM, Sims AQ, Riggs B (2015) Spatial reorganization of the endoplasmic reticulum during mitosis relies on mitotic kinase cyclin A in the early *Drosophila* embryo. *PLoS One* 10: e0117859

Bobinnec Y, Marcaillou C, Morin X, Debec A (2003) Dynamics of the endoplasmic reticulum during early development of Drosophila melanogaster. *Cell Motil Cytoskeleton* 54: 217-225

Bouvrais H, Chesneau L, Le Cunff Y, Fairbrass D, Soler N, Pastezeur S, Pécot T, Kervrann C, Pécréaux J (2021) The coordination of spindle-positioning forces during the asymmetric division of the *Caenorhabditis elegans* zygote. *EMBO Reports* 22: e50770

Brenner S (1974) The genetics of *Caenorhabditis elegans*. *Genetics* 77: 71-94

Brouhard GJ, Stear JH, Noetzel TL, Al-Bassam J, Kinoshita K, Harrison SC, Howard J, Hyman AA (2008) XMAP215 is a processive microtubule polymerase. *Cell* 132: 79-88

Cabral G, Laos T, Dumont J, Dammermann A (2019) Differential requirements for centrioles in mitotic centrosome growth and maintenance. *Dev Cell* 50: 355-366. e356

Chrétien D, Fuller SD, Karsenti E (1995) Structure of growing microtubule ends: two-dimensional sheets close into tubes at variable rates. *J Cell Biol* 129: 1311-1328

903 Conduit PT, Wainman A, Raff JW (2015) Centrosome function and assembly in animal
904 cells. *Nat Rev Mol Cell Biol* 16: 611-624
905
906 Diaz U, Bergman ZJ, Johnson BM, Edington AR, de Cruz MA, Marshall WF, Riggs B
907 (2019) Microtubules are necessary for proper Reticulon localization during mitosis.
908 *PLoS One* 14: e0226327
909
910 Enos SJ, Dressler M, Gomes BF, Hyman AA, Woodruff JB (2018) Phosphatase PP2A
911 and microtubule-mediated pulling forces disassemble centrosomes during mitotic exit.
912 *Biology Open* 7: bio029777
913
914 Farrell K, Jordan M, Miller H, Wilson L (1987) Phase dynamics at microtubule ends: the
915 coexistence of microtubule length changes and treadmilling. *J Cell Biol* 104: 1035-1046
916
917 Fong K-W, Choi Y-K, Rattner JB, Qi RZ (2008) CDK5RAP2 Is a Pericentriolar Protein
918 That Functions in Centrosomal Attachment of the γ-Tubulin Ring Complex. *Mol Biol Cell*
919 19: 115-125
920
921 Fygenson DK, Braun E, Libchaber A (1994) Phase diagram of microtubules. *Physical*
922 *Review E* 50: 1579-1588
923
924 Gao Q, Vermeulen BJ, Würtz M, Shin H, Erdogdu D, Zheng A, Hofer FW, Neuner A,
925 Pfeffer S, Schiebel E (2024) The structure of the γ-TuRC at the microtubule minus end–
926 not just one solution. *Bioessays* 46: 2400117
927
928 Gard DL, Kirschner MW (1987) A microtubule-associated protein from Xenopus eggs
929 that specifically promotes assembly at the plus-end. *J Cell Biol* 105: 2203-2215
930
931 Golden A, Liu J, Cohen-Fix O (2009) Inactivation of the *C. elegans* lipin homolog leads
932 to ER disorganization and to defects in the breakdown and reassembly of the nuclear
933 envelope. *J Cell Sci* 122: 1970-1978
934
935 Gould R, Borisy G (1977) The pericentriolar material in Chinese hamster ovary cells
936 nucleates microtubule formation. *J Cell Biol* 73: 601-615
937
938 Grego S, Cantillana V, Salmon ED (2001) Microtubule Treadmilling in Vitro Investigated
939 by Fluorescence Speckle and Confocal Microscopy. *Biophys J* 81: 66-78
940
941 Gudimchuk NB, McIntosh JR (2021) Regulation of microtubule dynamics, mechanics
942 and function through the growing tip. *Nat Rev Mol Cell Biol* 22: 777-795
943
944 Hachet V, Busso C, Toya M, Sugimoto A, Askjaer P, Gönczy P (2012) The nucleoporin
945 Nup205/NPP-3 is lost near centrosomes at mitotic onset and can modulate the timing of
946 this process in *Caenorhabditis elegans* embryos. *Mol Biol Cell* 23: 3111

Hamill DR, Severson AF, Carter JC, Bowerman B (2002) Centrosome maturation and mitotic spindle assembly in *C. elegans* require SPD-5, a protein with multiple coiled-coil domains. *Dev Cell* 3: 673-684

Hannak E, Oegema K, Kirkham M, Gönczy P, Habermann B, Hyman AA (2002) The kinetically dominant assembly pathway for centrosomal asters in *Caenorhabditis elegans* is γ-tubulin dependent. *J Cell Biol* 157: 591-602

Harris P (1975) The role of membranes in the organization of the mitotic apparatus. *Exp Cell Res* 94: 409-425

Hoffmann I (2021) Centrosomes in mitotic spindle assembly and orientation. *Curr Opin Struct Biol* 66: 193-198

Hu J, Rapoport TA (2016) Fusion of the endoplasmic reticulum by membrane-bound GTPases. *Semin Cell Dev Biol* 60: 105-111

Karabasheva D, Smyth JT (2019) A novel, dynein-independent mechanism focuses the endoplasmic reticulum around spindle poles in dividing *Drosophila* spermatocytes. *Sci Rep* 9: 1-13

Khodjakov A, Rieder CL (1999) The sudden recruitment of γ-tubulin to the centrosome at the onset of mitosis and its dynamic exchange throughout the cell cycle, do not require microtubules. *J Cell Biol* 146: 585-596

Kiyomitsu A, Nishimura T, Hwang SJ, Ansai S, Kanemaki MT, Tanaka M, Kiyomitsu T (2024) Ran-GTP assembles a specialized spindle structure for accurate chromosome segregation in medaka early embryos. *Nat Commun* 15: 981

Kuriyama R, Borisy GG (1981) Microtubule-nucleating activity of centrosomes in Chinese hamster ovary cells is independent of the centriole cycle but coupled to the mitotic cycle. *J Cell Biol* 91: 822-826

Lane HA, Nigg EA (1996) Antibody microinjection reveals an essential role for human polo-like kinase 1 (Plk1) in the functional maturation of mitotic centrosomes. *J Cell Biol* 135: 1701-1713

Laos T, Cabral G, Dammermann A (2015) Isotropic incorporation of SPD-5 underlies centrosome assembly in *C. elegans*. *Curr Biol* 25: R648-R649

Lee K, Rhee K (2011) PLK1 phosphorylation of pericentrin initiates centrosome maturation at the onset of mitosis. *J Cell Biol* 195: 1093-1101

Magescas J, Zonka JC, Feldman JL (2019) A two-step mechanism for the inactivation of microtubule organizing center function at the centrosome. *Elife* 8: e47867

Maheshwari R, Rahman MM, Drey S, Onyundo M, Fabig G, Martinez MA, Matus DQ, Müller-Reichert T, Cohen-Fix O (2023) A membrane reticulum, the centriculum, affects centrosome size and function in *Caenorhabditis elegans*. *Curr Biol* 33: 791-806. e797

Matthews LR, Carter P, Thierry-Mieg D, Kemphues K (1998) ZYG-9, a *Caenorhabditis elegans* protein required for microtubule organization and function, is a component of meiotic and mitotic spindle poles. *J Cell Biol* 141: 1159-1168

Megraw TL, Kao L-R, Kaufman TC (2001) Zygotic development without functional mitotic centrosomes. *Curr Biol* 11: 116-120

Megraw TL, Li K, Kao LR, Kaufman TC (1999) The centrosomin protein is required for centrosome assembly and function during cleavage in *Drosophila*. *Development* 126: 2829-2839

Mitchison T, Kirschner M (1984) Microtubule assembly nucleated by isolated centrosomes. *Nature* 312: 232-237

Mittasch M, Tran VM, Rios MU, Fritsch AW, Enos SJ, Ferreira Gomes B, Bond A, Kreysing M, Woodruff JB (2020) Regulated changes in material properties underlie centrosome disassembly during mitotic exit. *J Cell Biol* 219: e201912036

Moritz M, Braunfeld MB, Sedat JW, Alberts B, Agard DA (1995) Microtubule nucleation by γ-tubulin-containing rings in the centrosome. *Nature* 378: 638-640

Nakajo M, Kano H, Tsuyama K, Haruta N, Sugimoto A (2022) Centrosome maturation requires phosphorylation-mediated sequential domain interactions of SPD-5. *J Cell Sci* 135: jcs259025

O'Toole E, Greenan G, Lange KI, Srayko M, Müller-Reichert T (2012) The role of γ-tubulin in centrosomal microtubule organization. *PLoS One* 7: e29795

Ohta M, Zhao Z, Wu D, Wang S, Harrison JL, Gómez-Cavazos JS, Desai A, Oegema KF (2021) Polo-like kinase 1 independently controls microtubule-nucleating capacity and size of the centrosome. *J Cell Biol* 220: e202009083

Orso G, Pendin D, Liu S, Tosetto J, Moss TJ, Faust JE, Micaroni M, Egorova A, Martinuzzi A, McNew JA *et al* (2009) Homotypic fusion of ER membranes requires the dynamin-like GTPase atlastin. *Nature* 460: 978-983

Pelletier L, Ozlu N, Hannak E, Cowan C, Habermann B, Ruer M, Muller-Reichert T, Hyman AA (2004) The Caenorhabditis elegans centrosomal protein SPD-2 is required for both pericentriolar material recruitment and centriole duplication. *Curr Biol* 14: 863-873

Pimenta-Marques A, Bettencourt-Dias M (2020) Pericentriolar material. *Curr Biol* 30: R687-R689

Poteryaev D, Squirrell JM, Campbell JM, White JG, Spang A (2005) Involvement of the actin cytoskeleton and homotypic membrane fusion in ER dynamics in Caenorhabditis elegans. *Mol Biol Cell* 16: 2139-2153

Rahman M, Chang IY, Harned A, Maheshwari R, Amoateng K, Narayan K, Cohen-Fix O (2020) *C. elegans* pronuclei fuse after fertilization through a novel membrane structure. *J Cell Biol* 219: e201909137

Redemann S, Baumgart J, Lindow N, Shelley M, Nazockdast E, Kratz A, Prohaska S, Brugués J, Fürthauer S, Müller-Reichert T (2017) *C. elegans* chromosomes connect to centrosomes by anchoring into the spindle network. *Nat Commun* 8: 1-13

Rios MU, Bagnucka MA, Ryder BD, Ferreira Gomes B, Familiari NE, Yaguchi K, Amato M, Stachera WE, Joachimiak ŁA, Woodruff JB (2024) Multivalent coiled-coil interactions enable full-scale centrosome assembly and strength. *J Cell Biol* 223: e202306142

Rollins KR, Blankenship JT (2023) Dysregulation of the endoplasmic reticulum blocks recruitment of centrosome-associated proteins resulting in mitotic failure. *Development* 150: dev201917.

Schindelin J, Arganda-Carreras I, Frise E, Kaynig V, Longair M, Pietzsch T, Preibisch S, Rueden C, Saalfeld S, Schmid B (2012) Fiji: an open-source platform for biological-image analysis. *Nat Methods* 9: 676-682

Schlaitz AL (2014) Microtubules as key coordinators of nuclear envelope and endoplasmic reticulum dynamics during mitosis. *Bioessays* 36: 665-671

Srayko M, Kaya A, Stamford J, Hyman AA (2005) Identification and characterization of factors required for microtubule growth and nucleation in the early *C. elegans* embryo. *Dev Cell* 9: 223-236

Strome S, Powers J, Dunn M, Reese K, Malone CJ, White J, Seydoux G, Saxton W (2001) Spindle dynamics and the role of γ-tubulin in early *Caenorhabditis elegans* embryos. *Mol Biol Cell* 12: 1751-1764

Terasaki M (2000) Dynamics of the endoplasmic reticulum and Golgi apparatus during early sea urchin development. *Mol Biol Cell* 11: 897-914

Timothy LM, Li K, Kao L-R, Kaufman TC (1999) The Centrosomin protein is required for centrosome assembly and function during cleavage in *Drosophila*. *Development* 126: 2829-2839

Vasquez-Limeta A, Loncarek J (2021) Human centrosome organization and function in interphase and mitosis. *Semin Cell Dev Biol* 117: 30-41

Verde F, Labbé J-C, Dorée M, Karsenti E (1990) Regulation of microtubule dynamics by cdc2 protein kinase in cell-free extracts of Xenopus eggs. *Nature* 343: 233-238

Waterman-Storer CM, Sanger JW, Sanger JM (1993) Dynamics of organelles in the mitotic spindles of living cells: membrane and microtubule interactions. *Cell motil cytoskelet* 26: 19-39

Woodruff JB, Gomes BF, Widlund PO, Mahamid J, Honigmann A, Hyman AA (2017) The centrosome is a selective condensate that nucleates microtubules by concentrating tubulin. *Cell* 169: 1066-1077. e1010

Woodruff JB, Wueseke O, Hyman AA (2014)
Pericentriolar material structure and dynamics. *Philos Trans R Soc B: Biol Sci* 369: 20130459

Woodruff JB, Wueseke O, Viscardi V, Mahamid J, Ochoa SD, Bunkenborg J, Widlund PO, Pozniakovsky A, Zanin E, Bahmanyar S (2015) Regulated assembly of a supramolecular centrosome scaffold in vitro. *Science* 348: 808-812

Wueseke O, Zwicker D, Schwager A, Wong YL, Oegema K, Jülicher F, Hyman AA, Woodruff JB (2016) Polo-like kinase phosphorylation determines *Caenorhabditis elegans* centrosome size and density by biasing SPD-5 toward an assembly-competent conformation. *Biology open* 5: 1431-1440

Xie J, Najafi J, Nommick A, Lederer L, Salle J, Dmitrieff S, Lacroix B, Dumont J, Minc N (2025) Cell shape modulates mitotic spindle positioning forces via intracellular hydrodynamics. *Curr Biol*: S0960-9822(0924)01622-01621.

Zhang L, Ward JD, Cheng Z, Dernburg AF (2015) The auxin-inducible degradation (AID) system enables versatile conditional protein depletion in *C. elegans*. *Development* 142: 4374-4384

Zheng Y, Wong ML, Alberts B, Mitchison T (1995) Nucleation of microtubule assembly by a γ-tubulin-containing ring complex. *Nature* 378: 578-583

Zimmerman S, Chang F (2005) Effects of γ-tubulin complex proteins on microtubule nucleation and catastrophe in fission yeast. *Mol Biol Cell* 16: 2719-2733

1124 **Figure Legends**
1125

1126 **Figure 1: The spatial relationship between the centrosome, centriculum and peri-**
1127 **centrosomal microtubules.**
1128 **A)** Top panel: a *C. elegans* 1-cell embryo (strain OCF193) at metaphase expressing
1129 GFP::SP12 and PH domain::GFP (ER and plasma membrane markers, respectively; left
1130 panel and in green in merged panel) and TBA-1::RFP (microtubules; middle panel and
1131 in magenta in merged panel). Three types of microtubules are indicated: astral
1132 microtubules, which are nucleated at the centrosome and extend toward the cortex,
1133 spindle microtubules, which extend toward the chromosomes (not shown, but are
1134 located in the gap between the two half spindles), and peri-centrosomal microtubules,
1135 which accumulate in the vicinity of the centrosome but do not extend much past it. The
1136 two centricula flanking the spindle are indicated by yellow arrows in the left and merged
1137 images. Lower panel: *C. elegans* embryo (strain OCF176) at metaphase expressing
1138 GFP::SP12 (ER marker; green in merged panel) and GFP::SPD-5 (PCM marker;
1139 magenta in merged panel). Scale bar=10 μm.
1140 **B)** Schematic representation of the centrosome (PCM), with its area (light blue) defined
1141 by its outer perimeter (dark blue line); the centriculum, outlined by its inner and outer
1142 perimeters (dark orange lines; the area encompassed by the inner perimeter is defined
1143 as the centriculum "void", and the area enclosed by the outer perimeter of the
1144 centriculum is defined as the centriculum outer perimeter area, or COPA); and peri-
1145 centrosomal microtubule (pcMT) area (light green), defined by its outer perimeter (dark
1146 green).
1147 **C**, **D and E)** Quantification of void area (light orange), peri-centrosomal microtubules
1148 (green), PCM (blue) and COPA (dark orange) in 1-cell embryos from control RNAi
1149 treated worms. The strains and their relevant markers were as follows: Panel C:
1150 OCF181 (mCherry::SP12; GFP::TBA-2; n=26); Panel D: OCF176 (mCherry::SP12;
1151 GFP::SPD-5; n=22 for void area, n=24 for PCM, and n=23 for COPA; Panel E: OCF247
1152 (GFP::SPD-5; TBA-1:: tagRFP) n=20. Please refer to Fig. S1B for comparison with
1153 strain OCF240 (RFP::SPD-5; GFP::TBA-2). Statistical analyses: Panel C: p=0.0001 for
1154 void area vs pcMT area; p<0.0001 for void area vs COPA; p=0.0001 for pcMT area vs

1155 COPA. Panel D: p=0.0004 for void area vs PCM area; p<0.0001 for void area vs COPA;
1156 p=0.0002 for PCM area vs COPA. These analyses were done using Anova Kruskal-
1157 Wallis test. Panel E: p=0.0043 using Anova Mann-Whitney test. Error bars indicate
1158 mean and standard deviation.
1159 **F)** Schematic representation of the spatial relationship between the perimeters of the
1160 centriculum outer and inner perimeter (orange), peri-centrosomal microtubules (green)
1161 and the PCM (blue).
1162
1163 **Figure 2: Decrease in microtubule abundance or stability leads to a smaller**
1164 **centriculum and compression of the PCM.**
1165 **A)** Representative images of centricula from 1-cell embryos (OCF181) at metaphase
1166 expressing the SP12 ER marker fused to mCherry (mCherry::SP12; green in merged
1167 images) and α-tubulin fused to GFP (GFP::TBA-2; magenta in merged images), from
1168 worms treated with RNAi against a control (top row), *zyg-9* (middle row) or *tbg-1* RNAi
1169 (bottom row). Scale bar=5 μm.
1170 **B and C)** Quantification of GFP::TBA-2 peri-centrosomal microtubule area, void area
1171 and COPA, from embryos treated as shown in panel A. Panel B: n=26, 15, and 12 for
1172 control, *zyg-9* and *tbg-1* RNAi treatments, respectively. p< 0.0001 for control vs *zyg-9*
1173 and control vs *tbg-1* RNAi treatments using ordinary one-way ANOVA. Panel C: n=26,
1174 16 and 12 for control, *zyg-9* and *tbg-1* RNAi treatments, respectively. For void area: p<
1175 0.0001 for control vs *zyg-9* and control vs *tbg-1* RNAi treatments using Kruskal-Wallis
1176 test. For COPA: p< 0.0001 for control vs *zyg-9* RNAi and p=0.0072 for control vs *tbg-1*
1177 RNAi using ordinary one-way ANOVA. Error bars represent mean and standard
1178 deviation. Note that the values for control RNAi are the same as shown in Fig. 1C.
1179 **D)** Representative images of centricula and PCM from 1-cell embryos (OCF176) at
1180 metaphase expressing mCherry::SP12 (green in merged images) and the SPD-5 PCM
1181 protein fused to GFP (GFP::SPD-5; magenta in merged images), from worms treated
1182 with RNAi against a control (top row), *zyg-9* (middle row) or *tbg-1* (bottom row). Scale
1183 bar=5 μm.
1184 **E, F and G)** Quantification of GFP::SPD-5 area, amount and density (determined by
1185 SPD-5 total intensity divided (panel F) by SPD-5 area (panel E)) from embryos treated

1186 as shown in panel D. n=24, 12, and 16 for control, *zyg-9* and *tbg-1* RNAi treatments,
1187 respectively. For panel E: p<0.0001 for control vs *zyg-9* and for control vs *tbg-1* RNAi
1188 treatments using ordinary one-way ANOVA. Note that the control RNAi values for SPD-5
1189 area are the same as in Fig. 1D. Panel F: p=<0.0001 for control vs *zyg-9* and p=0.3290
1190 for control vs *tbg-1* RNAi treatments using ordinary one-way ANOVA. Panel G:
1191 p=<0.0001 for control vs *zyg-9* and for control vs *tbg-1* RNAi treatments using ordinary
1192 one-way ANOVA. Error bars indicate mean and standard deviation.
1193 **H)** GFP::SPD-5 density (as in panel G) as a function of void area (Fig. S1D) following
1194 control (magenta), *zyg-9* (purple), or *tbg-1* (pink) RNAi treatments. Linear regression
1195 was performed through all the datapoints. R^2=0.2624; slope was significantly different
1196 from 0 (p=0.0002).
1197
1198 **Figure 3: *spd-5* expansion mutant inhibits PCM expansion in the presence of wild**
1199 **type *spd-5***.
1200 **A)** Diagram depicting possible relationships between microtubules, the centriculum, and
1201 the PCM. See text for more detail.
1202 **B, C and D**) Representative images of centricula and PCM from 1-cell embryos at
1203 metaphase expressing mCherry::SP12 (green in merged images) and either (B) a
1204 *GFP::spd-5* transgene in the absence of endogenous protein (OCF187), (C) *GFP::spd-*
1205 *5^{exp}* in the absence of endogenous protein (OCF189), or (D) *GFP::spd-5^{exp}* in the
1206 absence of presence of endogenous protein (OCF189). The transgenic SPD-5 is shown
1207 in magenta in the merged images. In panels B and C, the endogenous gene was down-
1208 regulated using RNAi against *spd-5*; transgenes are codon modified such that they are
1209 insensitive to the RNAi treatment (Ohta *et al.*, 2021). Additional examples of images of
1210 embryos such as in panels C and D are shown in Fig S2A and B) Scale bar=5 µm.
1211 **E**) Representative images of PCM from 1-cell embryos at metaphase expressing
1212 endogenous RFP::SPD-5, and either transgenic GFP::SPD-5 wildtype (OCF201) or
1213 transgenic GFP::SPD-5^{exp} (OCF200). Scale bar= 5 µm.
1214 **F and G)** Quantification of areas occupied by endogenous RFP::SPD-5 and either
1215 transgenic GFP::SPD-5 (panel F) or GFP::SPD-5^{exp} (panel G) from images such as
1216 shown in panel E. n=11 and 13 for transgenic wild type and expansion mutant,

1217 respectively. $p<0.0001$ using unpaired t test. Error bars indicate mean and standard
1218 deviation.
1219 **H and I)** Quantification of protein amount (as reflected by total intensity) occupied by
1220 endogenous RFP::SPD-5 and either transgenic GFP::SPD-5 (panel H) or GFP::SPD-
1221 5^{exp} (panel I) in the areas quantified in panels F and G. $p=0.0004$ (panel H) and 0.0034
1222 (panel I), using Mann Whitney test.
1223
1224 **Figure 4: Microtubule nucleation remains unaffected in the presence of SPD-5**
1225 **expansion mutant**
1226 **A)** Representative images of peri-centrosomal microtubules and PCM from 1-cell
1227 embryos at metaphase expressing endogenous *tba-1::RFP* and either transgenic
1228 *GFP::spd-5* (OCF212) or transgenic *GFP::spd-5*^{exp} (OCF213), after control RNAi
1229 treatments. Scale bar=5 µm.
1230 **B, C and D)** Quantification of PCM area (panel B), amount of peri-centrosomal tubulin
1231 (panel C) and the area occupied by peri-centrosomal microtubules (pcMT; panel D) from
1232 control RNAi treated embryos such as shown in panel A. n=21 and n=29 for cells
1233 expressing transgenic wild type (WT) or expansion mutant (Exp) *spd-5*, respectively.
1234 $p<0.0001$ (panel B) and $p=0.3192$ (panel D) using unpaired t test, and $p=0.6400$
1235 (panel C) using Mann Whitney test. Error bars indicate mean and standard deviation.
1236 **E)** Quantification of area differential (pcMT area minus PCM area) derived from panels
1237 B and D. $p=0.0033$ using Mann Whitney test.
1238 **F)** Quantification of PCM area and pcMT area from the *klp-7* RNAi treated embryos
1239 using the same strains as in panels A-E (OCF212 and OCF213). n=20 and n=19 for
1240 strains expressing wild type or *spd-5*^{exp} transgenes, respectively. $p<0.0001$ for PCM
1241 areas and $p=0.4056$ for pcMT areas, using ordinary one-way ANOVA. Error bars
1242 indicate mean and standard deviation.
1243 **G)** Quantification of area differential (pcMT- PCM, as in panel E) derived from pcMT and
1244 PCM areas (panel F) in *klp-7* RNAi treated embryos. $p=0.0014$ using the Mann Whitney
1245 test.
1246

1247 **Figure 5: Centriculum size correlates with the position of peri-centrosomal**
1248 **microtubules, not the PCM**.
1249 **A)** Schematic representation of the spatial relationship between the perimeters of the
1250 centriculum (orange), PCM (blue) and the peri-centrosomal microtubules (green). (i) In
1251 the presence of *spd-5*^{exp} mutant, the area of the PCM, but not the peri-centrosomal
1252 microtubules, decreases, and thus the distance between the edges of the two structures
1253 should increase. (ii) When considering how the centriculum size, and specifically the
1254 area bound but the centriculum's inner perimeter (the void area), is affected by the
1255 presence of *spd-5*^{exp} mutant, two possibilities emerge: the edge of the void area follows
1256 the PCM (left) or the peri-centrosomal microtubules (right). See text for more detail.
1257 **B)** Example of centricula and peri-centrosomal microtubules from 1-cell embryos
1258 expressing GFP::SP12 (green in merged image) and TBA-1::RFP (magenta in merged
1259 image) and either wild type (OCF214) or *spd-5*^{exp} (OCF215) transgenes, following
1260 control or *klp-7* RNAi treatments. Scale bar=5 μm.
1261 **C and D)** Quantification of pcMT areas (panel C) and void areas (panel D) from control
1262 RNAi treated embryos as in panel B. n=19 and n=15 for transgenic wild type and spd-
1263 5^{exp} expressing strain, respectively. $p<0.0001$ for pcMT area comparison using Mann
1264 Whitney test, and $p<0.0001$ for void area comparison using unpaired t test. Error bars
1265 indicate mean and standard deviation.
1266 **E)** Quantification of area differential (pcMT area minus void area) derived from area
1267 values shown in panels C and D and Fig S3C. n=19, 15, 20, 23 for control RNAi, wild
1268 type and *spd-5*^{exp} transgenes and *klp-7* RNAi, wild type and *spd-5*^{exp} transgenes. p-
1269 values, from left to right, were 0.5653, 0.013, 0.2353 and 0.9945, using ordinary one-
1270 way ANOVA. Error bars indicate mean and standard deviation.
1271 **F)** Representative images of centricula and PCM from 1-cell embryos at metaphase
1272 expressing *mCherry::SP12* (green in merged images) and either *GFP::spd-5* (OCF187)
1273 or *GFP::spd-5*^{exp} (OCF189) transgenes (magenta in merged images), following control
1274 or *klp-7* RNAi treatment. White arrow in enlarged image points to a gap between the
1275 centriculum and SPD-5. Scale bar=5 μm.
1276 **G and H)** Quantification of PCM area (panel G) and void area (panel H) from 1-cell
1277 metaphase embryos as shown in panel F, following control or *klp-7* RNAi treatment.

1278 n=12 all conditions except n=16 for *spd-5*^{exp} transgene following control RNAi. For PCM
1279 area, p<0.0001 for all pairwise comparisons as determined by ordinary one-way
1280 ANOVA. For void area, p-values, from left to right, are 0.6133, <0.0001, <0.0001 and
1281 0.9999, as determined by ordinary one-way ANOVA. Error bars indicate mean and
1282 standard deviation.
1283 **I)** Quantification of the area differential (PCM area minus void area) derived from area
1284 values shown in panels G and H. p-values, as determined by ordinary one-way
1285 ANOVA, were <0.0001, except for WT vs Exp, control RNAi, where the p-value was
1286 p=0.0003. Error bars indicate mean and standard deviation.
1287
1288 **Figure 6: Spatial relationship between the centriculum and the PCM using an**
1289 **endogenously tagged *spd-5* in the presence of *spd-5*^{exp} mutant**
1290 **A)** Representative images of centricula and PCM from 1-cell embryos at metaphase
1291 expressing RFP-tagged endogenous *spd-5* (RFP::SPD-5, in magenta) and GFP::SP12
1292 (in green) in strains expressing either wild type (OCF234) or *spd-5*^{exp} (OCF233)
1293 transgenes, following control or *klp-7* RNAi treatment. Scale bar=5 µm.
1294 **B, C and D)** Quantification of SPD-5 amount, PCM areas and void areas from 1-cell
1295 metaphase embryos treated as shown in panel A. n=16 and 11 for wild type and *spd-*
1296 *5*^{exp} transgenes treated with control RNAi, and n=20 and n=16 for wild type and *spd-5*^{exp}
1297 transgenes treated with *klp-7* RNAi. p-values, from left to right, were as follows: panel B:
1298 <0.0001, 0.1795, 0.3578 and <0.0001, as determined by ordinary one-way ANOVA;
1299 panel C: 0.0018, 0.0023, 0.0286 and <0.0001, as determined by Kruskal-Wallis test;
1300 panel D: 0.0547, and the rest were <0.0001, as determined by ordinary one way
1301 ANOVA. Error bars indicate mean and standard deviation.
1302 **E)** Quantification of the area differential (PCM area minus void are) derived from data
1303 shown in panels C and D. p-values, as determined by ordinary one-way ANOVA, were
1304 <0.0001 except for p=0.0001 for wild type, control vs *klp-7* RNAi. Error bars indicate
1305 mean and standard deviation.
1306 **F)** Diagram illustrating the effect of the spd-5^{exp} transgene on the centriculum (orange),
1307 peri-centrosomal microtubules (green) and PCM (blue). See text for more detail.
1308

1309 **Figure 7: Porousity of the centriculum facing the cortex**.
1310 **A)** Representative images of 1-cell *C. elegans* embryos expressing mCherry::SP12 to
1311 visualize the centriculum and GFP::TBA-2 (α-tubulin) to visualize microtubules (strain
1312 OCF181) at prophase (left side) and metaphase (right side). Note that at prophase,
1313 microtubules are excluded from the nucleoplasm, and that in metaphase, the density of
1314 spindle microtubules is greater than astral microtubules. Scale bar=10 µm.
1315 **B)** Diagram depicting the centriculum (in orange) fused to the two pronuclei (brown
1316 lines) at a metaphase 1-cell embryo. Chromosomes (in red) and the cortex (black line)
1317 are also indicated. The areas analyzed for pore size are shown as blue (chromosome
1318 facing) and green (cortex facing) trapezoids. A central fiducial (in pink) that is equidistant
1319 (pink arrows) to the areas analyzed is also shown.
1320 **C)** Cortical and pronuclear centriculum segments based on FIB-SEM data (Maheshwari
1321 *et al.*, 2023) from two centricula, shown side by side. The images were taken from the
1322 central fiducial. Scale bar=200 nm.
1323 **D)** Binned frequency distribution of holes present on the cortical side (in green) and
1324 chromosome side (in blue) of centricula in 1-cell metaphase embryos. Bin size range,
1325 as hole area, is shown on the x-axis. n=308 and 507 for chromosomal and cortex side
1326 holes, respectively, each containing data pooled from 6 images taken from 3 centricula
1327 (2 images per centriculum).
1328 **E)** Binned frequency distribution of the percentage of total open area per hole size
1329 range, for holes on the cortical side (green) and the pronuclear side (blue) using the
1330 same data as in panel D.
1331
1332 **Figure 8:**
1333 **A)** Diagram depicting the angle of a microtubule (green line) passing through the
1334 centriculum (in orange) relative to the radial vector (dashed purple line). The actual
1335 measurement was done between the microtubule and the tangent line (dashed black
1336 line) and the value obtained was subtracted from 90 to obtain the angle to the radial
1337 vector, which is perpendicular to the tangent line.
1338 **B)** Quantification of angles between of stopped (in orange) and continuing (in cyan)
1339 microtubule and radial vector for astral (cortex-facing) and spindle (chromosome-facing)

microtubules. Based on EM tomography data (Redemann *et al.*, 2017). p=0.0029 (for cortex-facing) and 0.0018 (chromosome-facing) using one-way ANOVA with multiple comparisons. Error bars indicate mean and standard deviation.

C) Left panel: Representative images of a segmented area based on FIB-SEM data (Maheshwari *et al.*, 2023) from the pronuclear side of two prometaphase centricula (in yellow), visualized from the center of the centrosome. Right panel: the same images with segmentation of nuclear membrane remnants (in green) that are between the centriculum and the prometaphase chromosomes (not shown). Scale bar=200 nm.

D) Areas of possible contact (indicated by red arrows) between a prometaphase centriculum (in yellow) and remnants of the nuclear membrane (in green) based on FIB-SEM data (Maheshwari *et al.*, 2023). In this image, the centrosome is to the upper right side while the chromosomes are to the lower left side.

E) Two 1-cell embryos expressing mCherry::SP12 and GFP::TBA-2 from worms in which atlastin was downregulated using an auxin-inducible degron (AID) system (OCF183, see (Maheshwari *et al.*, 2023)). Red arrows point to sites where a centriculum has fused to a single pronucleus. Green arrows point to sites where a centriculum has fused to both pronuclei. The same arrows are shown in the bottom panels, where they are adjacent to sites where spindle microtubules extend into the pronuclei. Blue asterisks indicate pronuclei that fuse to only one centriculum. The enlarged areas show sites of centriculum-pronuclear fusion. Note that unlike the wild type situation (Fig 7A), under these conditions the two pronuclei fail to align and do not form extensive pronuclear interfacial contacts. Scale bar=10 μm.

Figure 1

A

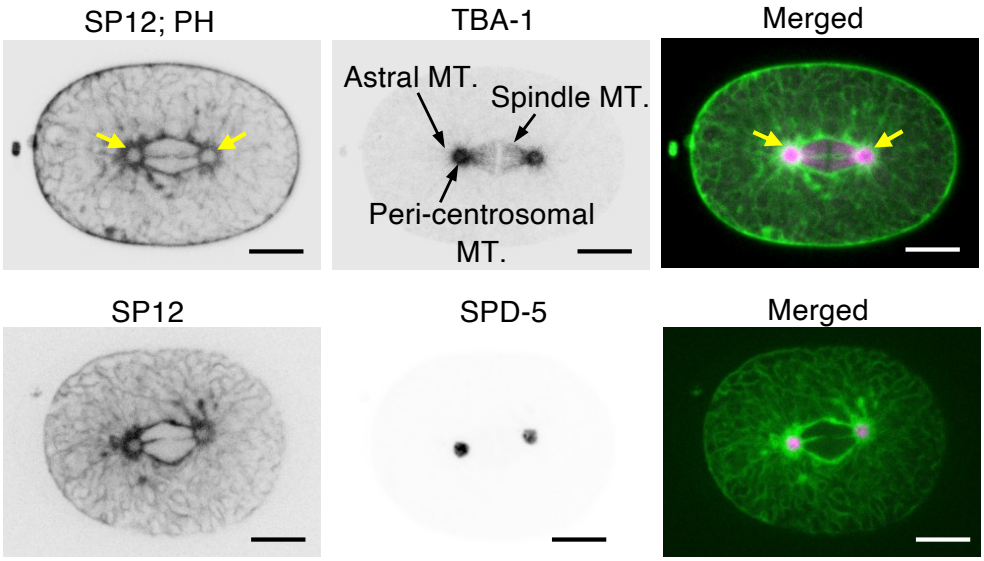

B

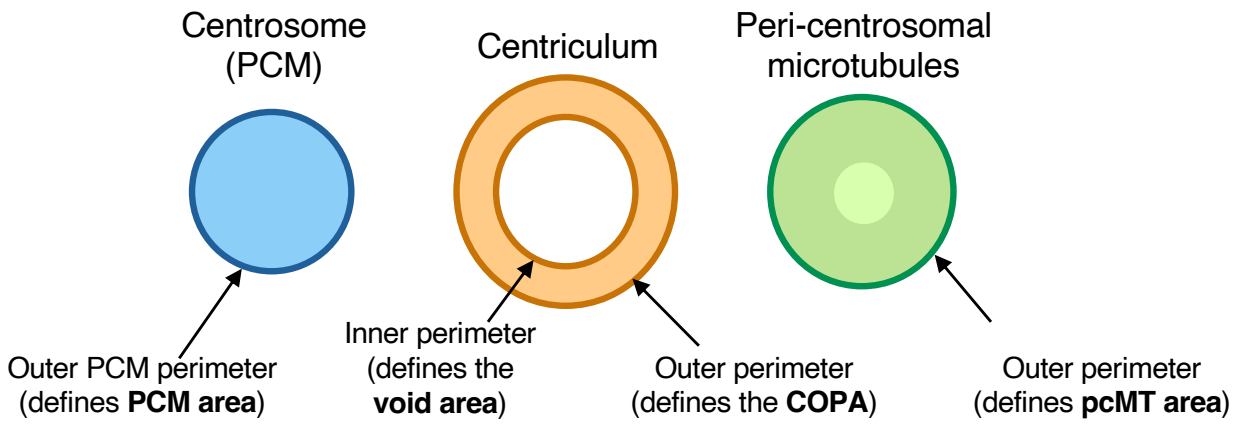

C

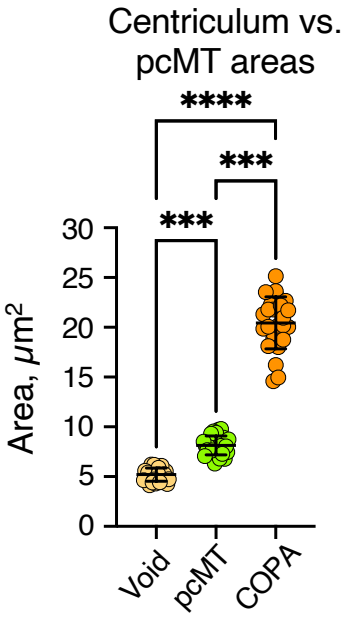

D

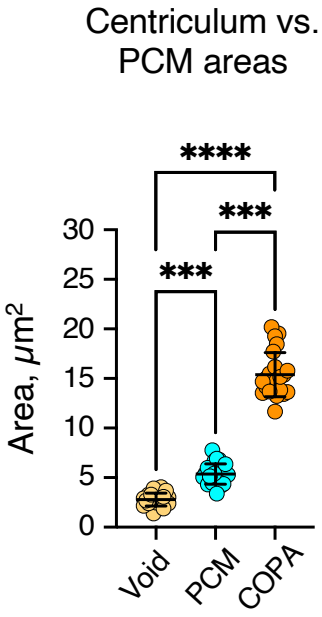

E

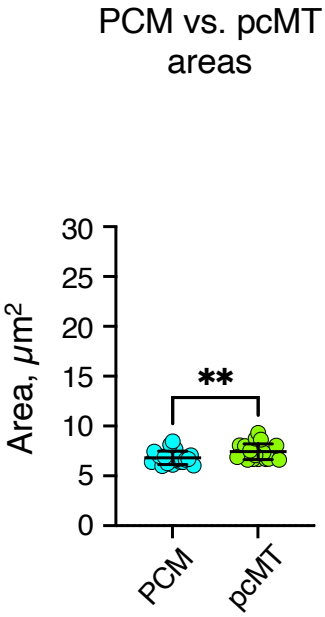

F

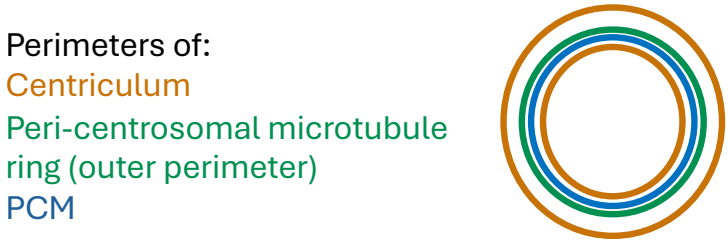

Figure 2

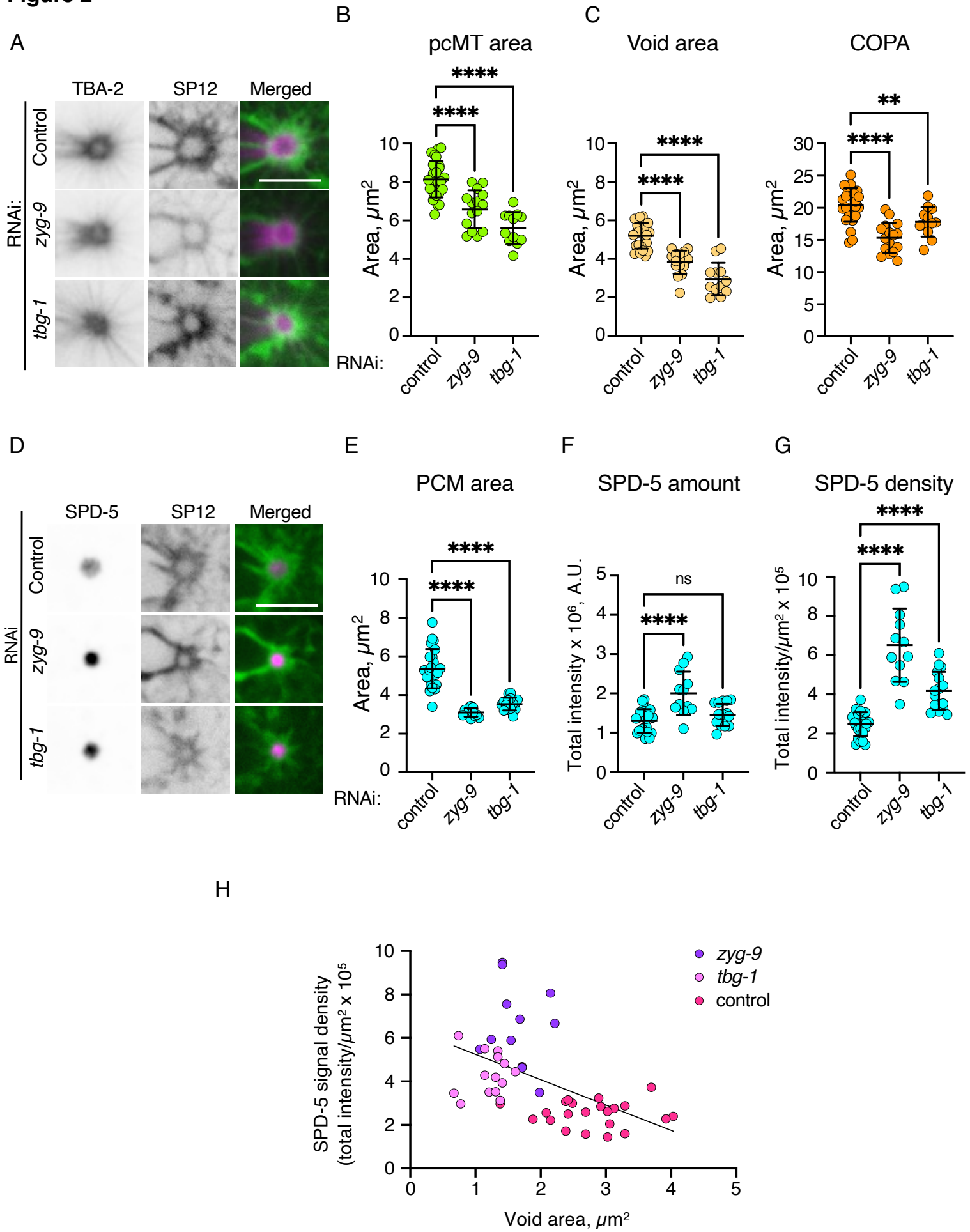
A
TBA-2
SP12
Merged
RNAi:
Control
zyg-9
tbg-1
B
pcMT area
Area, μm²
RNAi:
control
zyg-9
tbg-1
****
****
C
Void area
Area, μm²
****
****
COPA
Area, μm²
**
****
D
SPD-5
SP12
Merged
RNAi
Control
zyg-9
tbg-1
E
PCM area
Area, μm²
****
****
F
SPD-5 amount
Total intensity x 10⁶, A.U.
ns
****
G
SPD-5 density
Total intensity/μm² x 10⁵
****
****
H
SPD-5 signal density
(total intensity/μm² x 10⁵
Void area, μm²
zyg-9
tbg-1
control

Figure 3

A

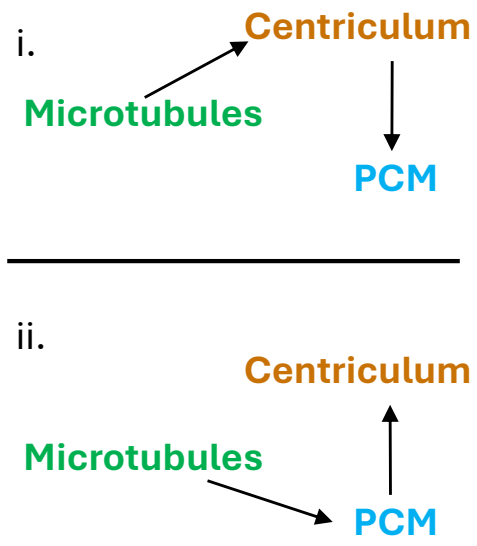

B

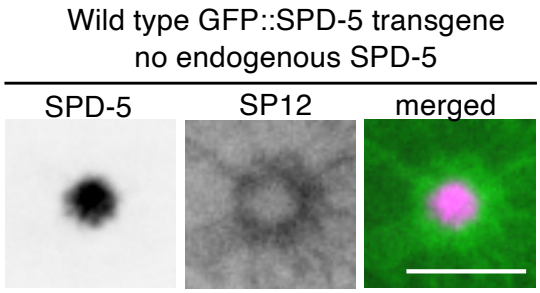

C

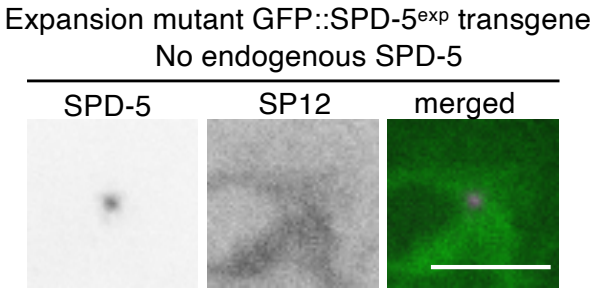

D

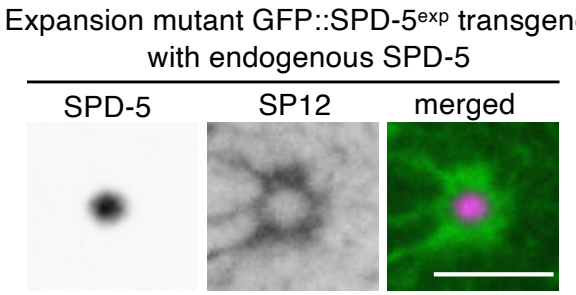

E

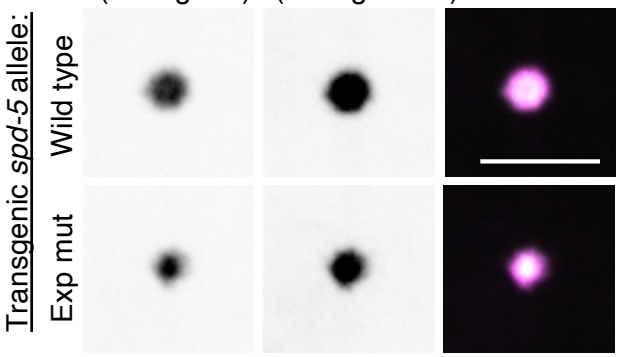

F

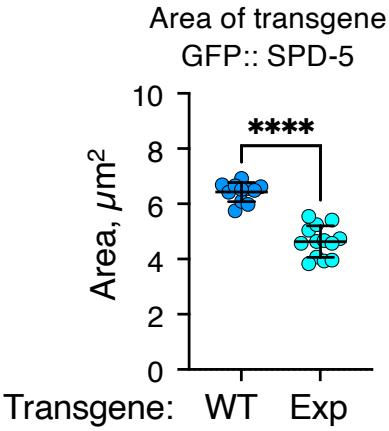

G

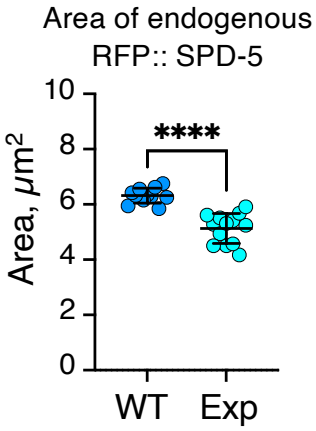

H

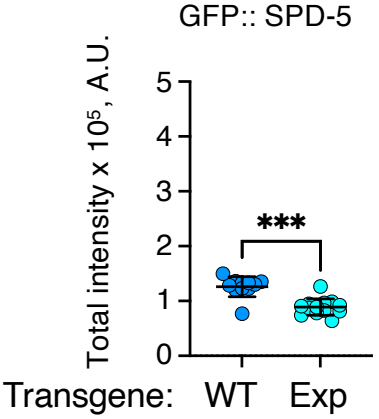

I

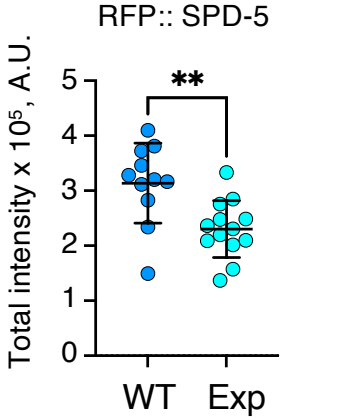

Figure 4

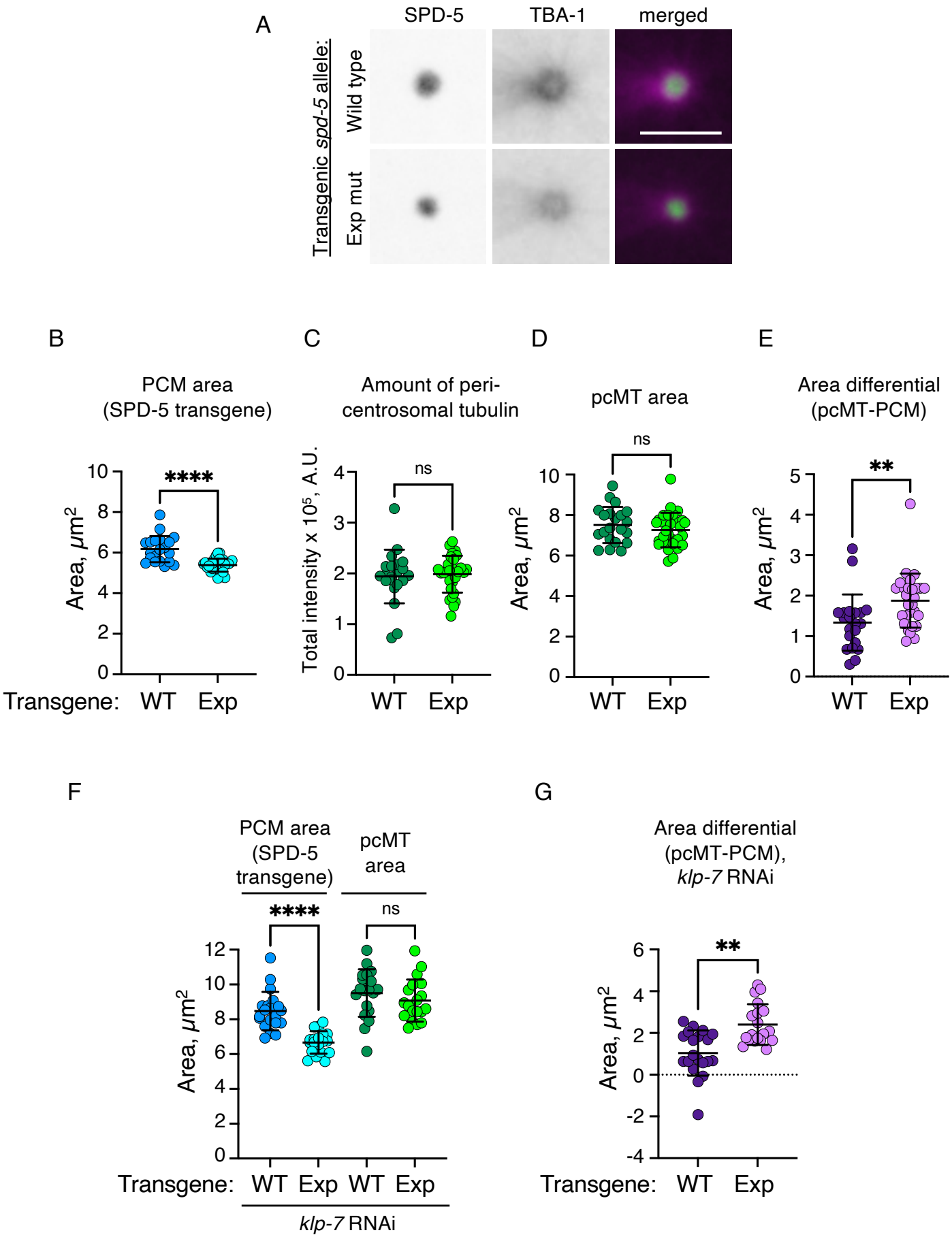
A
SPD-5
TBA-1
merged
Transgenic spd-5 allele:
Wild type
Exp mut
B
PCM area
(SPD-5 transgene)
Area, μm2
****
Transgene: WT Exp
C
Amount of peri-
centrosomal tubulin
Total intensity x 10^5, A.U.
ns
WT Exp
D
pcMT area
Area, μm2
ns
WT Exp
E
Area differential
(pcMT-PCM)
Area, μm2
**
WT Exp
F
PCM area
(SPD-5
transgene)
pcMT
area
Area, μm2
****
ns
Transgene: WT Exp WT Exp
klp-7 RNAi
G
Area differential
(pcMT-PCM),
klp-7 RNAi
Area, μm2
**
Transgene: WT Exp

Figure 5

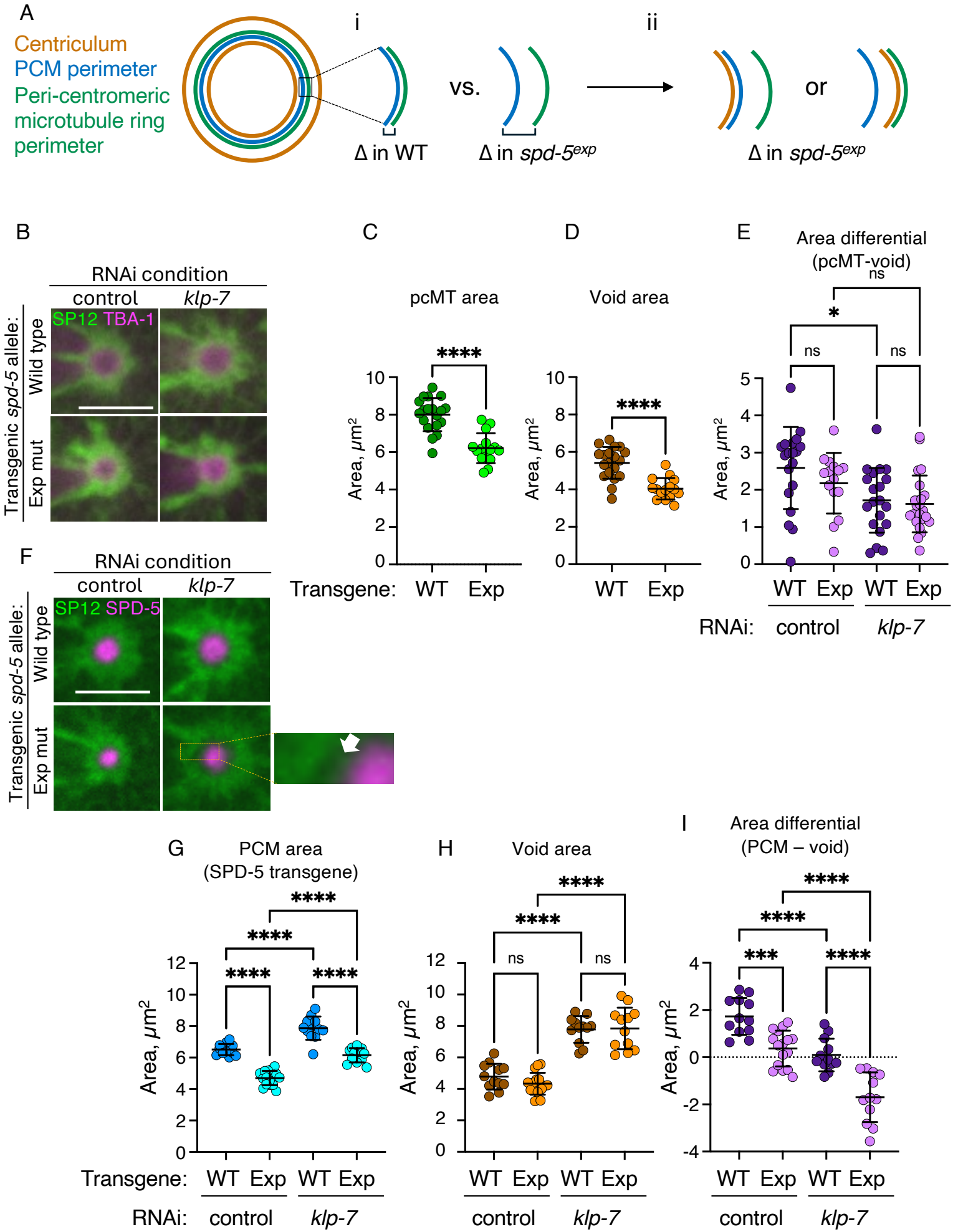
A
Centriculum
PCM perimeter
Peri-centromeric microtubule ring perimeter
i
ii
vs.
or
Δ in WT
Δ in spd-5exp
Δ in spd-5exp
B
RNAi condition
control
klp-7
Transgenic spd-5 allele:
Wild type
Exp mut
SP12 TBA-1
C
pcMT area
Area, μm2
Transgene: WT Exp
D
Void area
E
Area differential (pcMT-void)
ns
*
RNAi: control klp-7
F
SP12 SPD-5
G
PCM area (SPD-5 transgene)
H
Void area
I
Area differential (PCM – void)
***
****

Figure 6

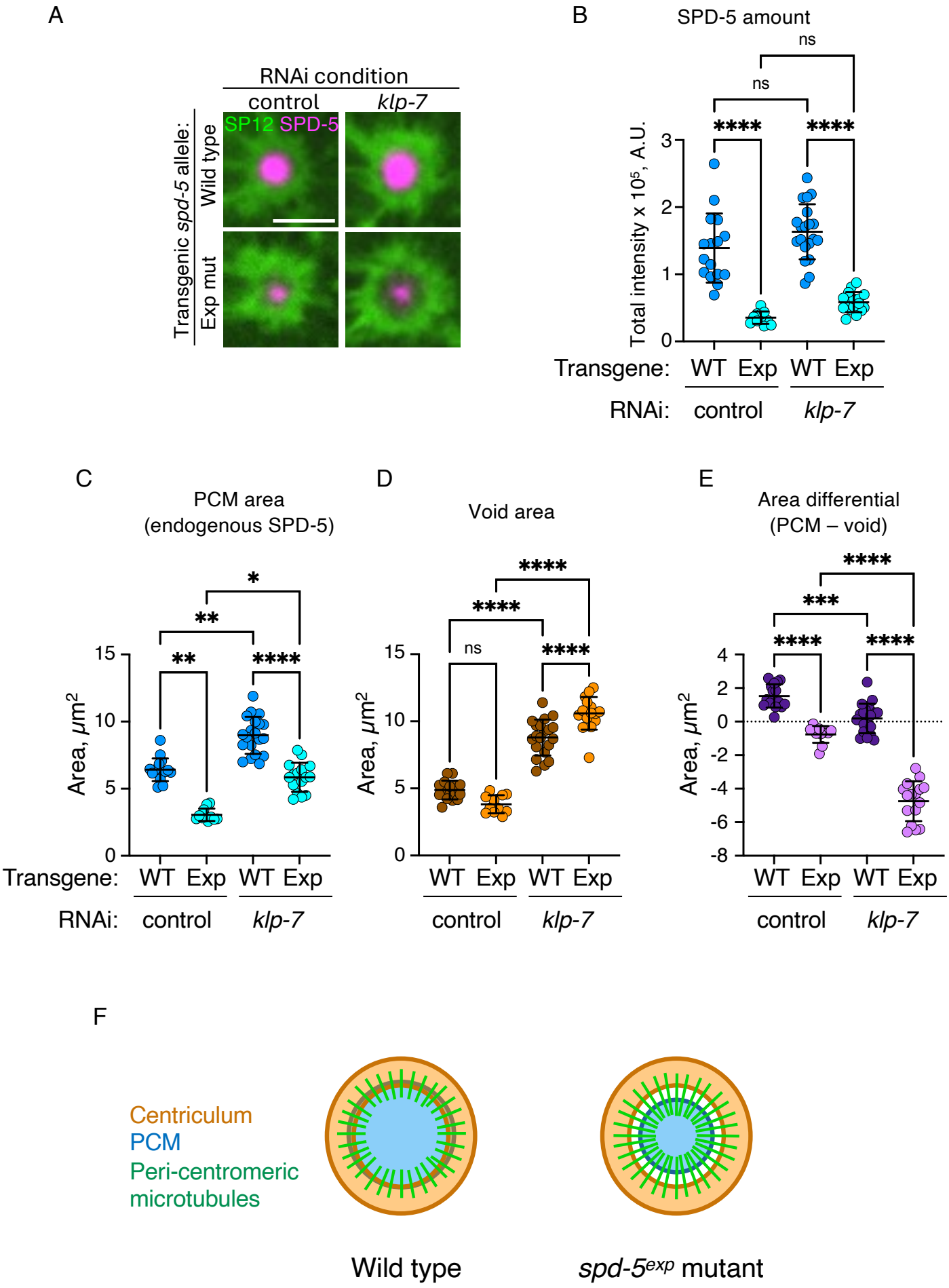
A
RNAi condition
control
klp-7
SP12 SPD-5
Transgenic spd-5 allele:
Wild type
Exp mut
B
SPD-5 amount
ns
ns
****
****
Total intensity x 10^5, A.U.
Transgene: WT Exp WT Exp
RNAi: control klp-7
C
PCM area
(endogenous SPD-5)
*
**
**
****
Area, μm²
Transgene: WT Exp WT Exp
RNAi: control klp-7
D
Void area
****
****
ns
****
Area, μm²
WT Exp WT Exp
control klp-7
E
Area differential
(PCM – void)
****
***
****
****
Area, μm²
WT Exp WT Exp
control klp-7
F
Centriculum
PCM
Peri-centromeric
microtubules
Wild type
spd-5exp mutant

Figure 7

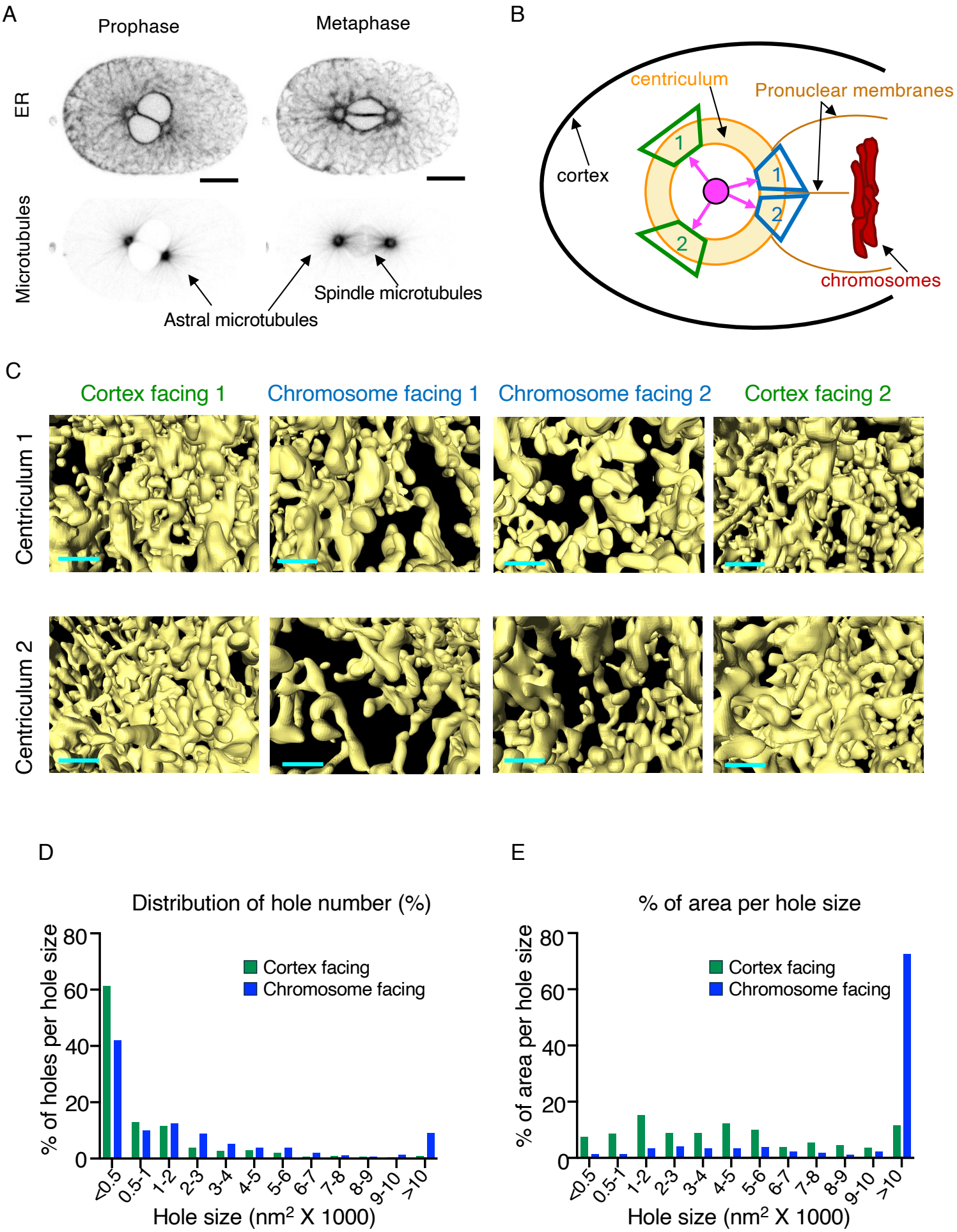
A
Prophase
Metaphase
ER
Microtubules
Astral microtubules
Spindle microtubules
B
centriculum
Pronuclear membranes
cortex
1
2
1
2
chromosomes
C
Cortex facing 1
Chromosome facing 1
Chromosome facing 2
Cortex facing 2
Centriculum 1
Centriculum 2
D
Distribution of hole number (%)
% of holes per hole size
Cortex facing
Chromosome facing
Hole size (nm² X 1000)
E
% of area per hole size
% of area per hole size
Cortex facing
Chromosome facing
Hole size (nm² X 1000)

Figure 8

A

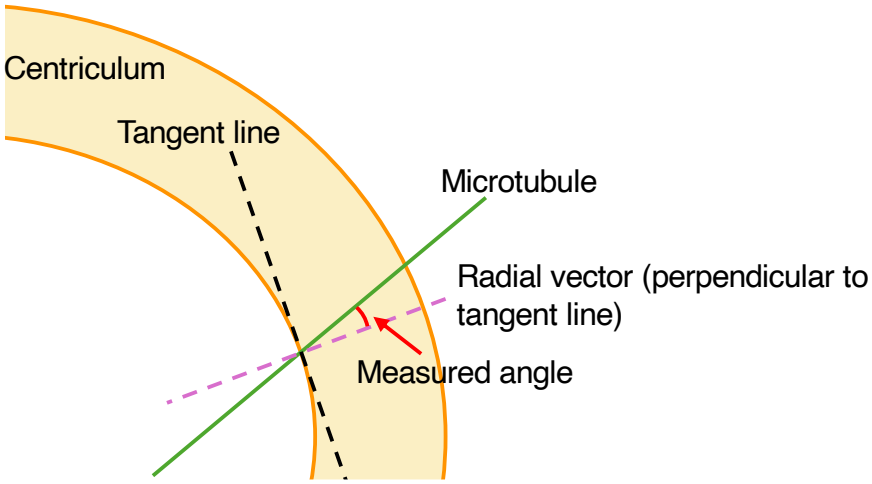

B

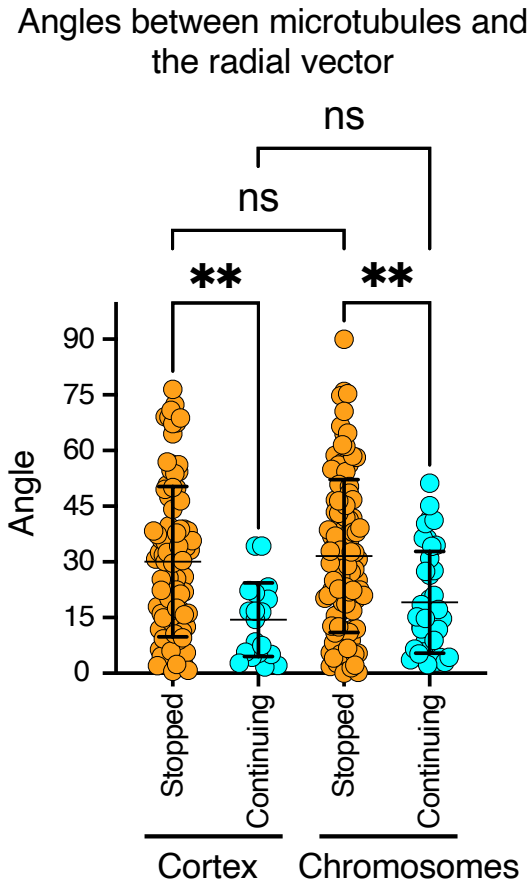

C

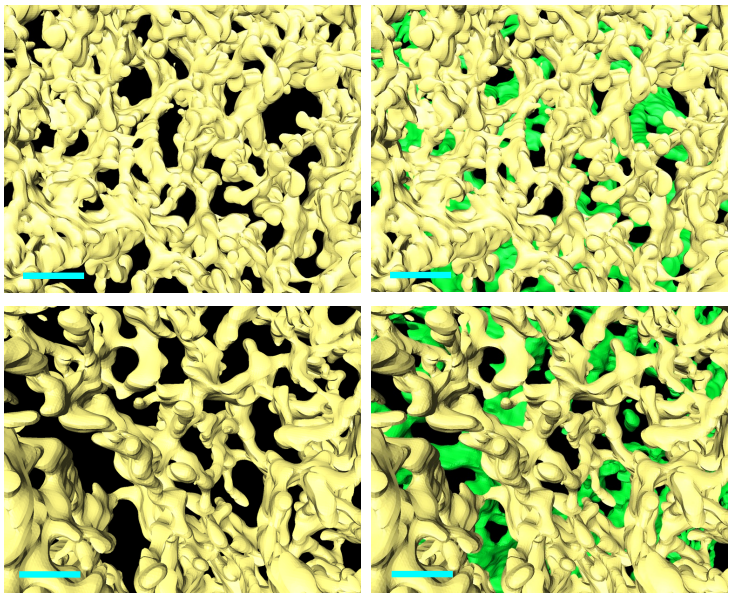

D

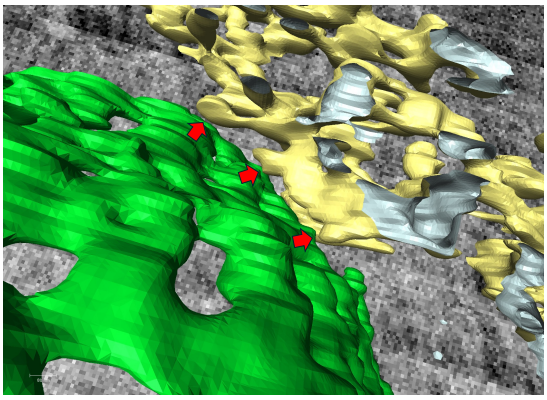
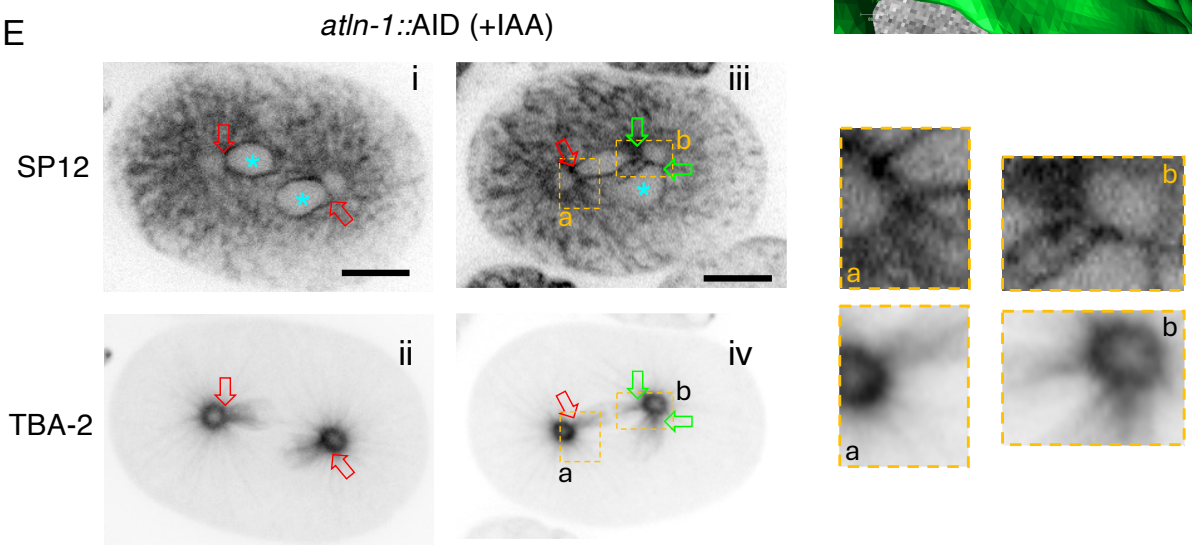
E